Concrete self-healing performance using surface roughness parameters: Metrological approach

Amir Sidiq [a], Sujeeva Setunge [a], Pratheep Kumar Annamalai [c,d], Rebecca J. Gravina [b], Filippo Giustozzi [a,*]

[a] STEM | School of Engineering, Royal Melbourne Institute of Technology (RMIT University), 376-392 Swanston St, Melbourne, VIC, 3001, Australia
[b] School of Civil Engineering, The University of Queensland, Brisbane QLD, 4072, Australia
[c] School of Agriculture and Food Sustainability, The University of Queensland, Brisbane QLD, 4072, Australia
[d] Centre for Future Materials, University of Southern Queensland, Toowoomba, QLD 4350, Australia

ARTICLE INFO

ABSTRACT

Traditional test methods for evaluating concrete self-healing performance, such as scanning electron microscopy, ultrasonic waves including velocity pulse and emissions and x-ray imaging have limited accuracy resulting from the damages during the sample preparation and capability of the instruments. Very limited work has been performed to date to conduct non-destructive evaluations using non-contact test methods, hence obtaining three-dimensional images that can evaluate the self-healing performance in cementitious materials. This study meteorological instruments to obtain three-dimensional surface profiles without any external impacts that could potentially cause damage to the concrete surface has been used. The study aims evaluate the healing efficiency and performance of the crack at different time intervals for 28 days by using different healing agents such as microcapsules, cellulose fibre and applying sodium silicate directly on the developed crack. Healing efficiency and performance assessment is conducted through the maximum visualisation featuring, crack width, depth healed product from the contact angle. Metrological selective roughness parameters such as Sa, Sq, Vvv and Smr2 values are also used to evaluate the self-healing performance at various time intervals. A comparison of the numerically obtained data, both individually and from different surface roughness parameters, indicates that crack healing occurrences can be observed when utilizing different healing agents.

1. Introduction

Concrete is employed as a fundamental material for large infrastructures owing to its commendable fire resistance, compressive strength, and straightforward casting process. With the exponential growth of the global population and industrialization, concrete is now extensively utilized in applications such as highways, marine structures, and wastewater treatment facilities [1]. Statistics show that cement production in major cement manufacturing countries was 2.88 billion tonnes in 2010. By 2016, this figure had risen to 3.54 billion tonnes [2] and the expected growth is projected to reach approximately 4.86 billion tonnes by 2030 [3]. Contrastingly, one drawback of cement-based products is the occurrence of cracking. Within cementitious materials, micro-cracks form as a result of various physical and chemical interactions in the cementitious matrix and on its surfaces throughout the lifespan of the concrete structure. In modern structures, concrete is often exposed to more rigorous environmental and mechanical conditions than in the past.

This, combined with the inherent heterogeneity of the concrete, contributes to a lack of crack width. Consequently, this provides a pathway for undesirable particles such as sulphates and chlorides to infiltrate the cementitious materials, leading to the deterioration of the reinforced structure. This issue is considered one of the most significant challenges faced by reinforced structures, as it significantly impacts their mechanical properties and thus compromises the overall durability of the concrete structure [4,5]. Therefore, various crack repair techniques such as epoxy injection, gravity filling, and grouting are regularly used, while the cost of such maintenance is approximately double compared to the cost of concrete manufacturing [6]. While, such maintenance is mainly to prevent the concrete structure from further deterioration, hence retaining the durability of the structure, however it is not responsible for recovering the strength of the concrete structure [7]. Researchers have put significant effort into focusing on reducing the probability of crack occurrence in the cementitious matrix to attain higher structural performance.

In reflection of the significant quantity of cracks in cementitious materials and their deterioration effects on the structural integrity, researchers have investigated the phenomenon of self-healing in cementitious materials through different healing technologies such as polymers, bacterial and chemical compounds to seal and heal the cracks at the macro and micro level [8]. The contribution of polymers as a healing agent is considered a non-compatible material with cementitious materials due to the lack of adhesion between the polymers and the concrete crack walls [9,10]. Researchers have also employed bacillus bacteria as a healing agent, and the production of healing products has been relatively achieved through calcium carbonate production. This can be formed through either the ureolytic or denitrification process, although there are uncertainties regarding the consistent production of the healing product [11,12]. On the other hand, chemical compounds like Magnesium Oxide are utilized as a healing agent to produce magnesium carbonate. However, it's important to note that this healing agent is only applicable in water embankments due to the necessity of water content to facilitate the completion of the chemical reaction [13]. Sodium Silica is also employed as a healing agent, involving a chemical reaction between sodium silica and the calcium hydroxide in the cementitious matrix. This reaction leads to the formation of newly created Calcium-Silica-Hydrate (C–S–H) products [14,15], as shown in equations (1) and (2).

The following reactions show the interaction between sodium silica and calcium hydroxide and the formation of Calcium-Silica-Hydrate product.

$$Na_2O \cdot SiO_2 + Ca(OH)_2 \rightarrow x(CaO \cdot SiO_2) \cdot H_2O + Na_2O \tag{1}$$

$$x(CaO \cdot SiO_2) \cdot H_2O + Na_2O + CO_2 \rightarrow CaCO_3 + SiO_2 + 2NaOH \tag{2}$$

Amongst the various healing agents available for crack healing in cementitious materials, test methods for evaluating the healing performance and efficiency also play significant roles. Traditionally, researchers have used mechanical tests such as compression and flexural test methods to evaluate healing efficiency. It has been demonstrated that there is a high degree of test variation in those test methods. This variability can be attributed to the heterogeneity of the cementitious materials and the aggregates/sand particles, which can result in variations within the microstructure matrix [16]. Therefore, researchers have essentially limited using the mechanical test methods for concrete self-healing evaluations and have been attracted to use of the non-destructive test methods for crack healing evaluations. One of the most common non-destructive tests used for concrete self-healing applications is the Ultrasonic Velocity Pulse (UVP) test due to the simple operation of the testing mechanism. The UVP is used to evaluate the self-healing through the speed of the pressure wave passing through the concrete specimen from one transducer to the other (generally at 54 kHz) [17], which can then be used to back-calculate the stiffness of the material by using ASTM-C597 [18]. However, the certainty of the results is constrained by the heterogeneity of the cementitious materials, as mentioned earlier. Consequently, an inaccurately high speed of the pressure wave is recorded, which can impact the overall testing results [19]. Other researchers have explored the use of Acoustic Emission (AE) as an alternative non-destructive test method to assess healing efficiency in cement-based products. During the loading process and the formation of cracks, elastic waves are generated. These waves are then detected by transducers, enabling the determination of the location of the cracks [20,21]. UVP and AE prove to be effective test methods for identifying discontinuities within concrete samples. However, they offer limited information regarding crack width and the closure of cracks during the healing process. As a result, researchers commonly employ the scanning electron microscope (SEM) to capture topological, two-dimensional (2D) images that depict the closure of crack widths during the healing progress. This enables a more comprehensive evaluation of self-healing efficiency [22]. It's crucial to acknowledge that the process of obtaining SEM images involves subjecting the sample to high vacuum pressure. This can potentially result in additional damage or alteration to the sample's surface texture, potentially affecting its topological properties and leading to inaccurate results. Additionally, SEM images provide two-dimensional representations, making it possible to assess crack width but challenging to gather information about crack depth. To address these limitations, researchers have explored the use of non-destructive test methods in conjunction with non-contact test methods that have minimal environmental impact, such as avoiding the use of high vacuum pressure in SEM. One promising approach gaining traction is the utilization of X-ray micro computed tomography (CT). This method is considered highly non-destructive and non-contact, making it ideal for evaluating self-healing efficiency in cementitious materials. Micro CT offers extensive qualitative and quantitative analysis capabilities, providing valuable insights into self-healing mechanisms [23,24]. However, there are notable drawbacks of this test method as well, among which 1) Preparing the concrete sample for the micro-stage of the micro CT instrument can be intricate and may not perfectly represent a standard concrete sample. This process may involve multiple alterations, potentially resulting in damage to the sample [25]. And, 2) the CT imaging parameters somehow subjective set up and the noise ratio which impacts the resolution of the image and the capacity of the x-ray energy to pass through during the scanning process [26].

An alternative non-destructive, non-contact test method is metrological surface texture roughness testing, commonly utilized in microelectronics fabrication. This method offers distinct advantages: 1) metrological tests can be undertaken at ambient temperature, 2) the sample preparation is straightforward and does not require cutting and/or drilling, and 3) this type of test provides high-

resolution data, enabling the assessment of surface features like peaks and valleys. A paradigm of metrology with the definition of the fundamental parameters and principles for the metrological application together with the descriptive surface morphology of concrete materials has been evaluated in past studies [27,28]. Alternatively, some researchers have employed metrological methods to assess surface roughness in concrete for various applications (i.e. evaluation of the surface roughness parameters for the effectiveness of water-cement ratio and compressive strength sensitivity [29], characterization of the surface treatment on the concrete surface [30] and surface fracture of cementitious materials [31]), however the use of the 3D metrology in self-healing applications remains limited. Metrological parameters, particularly those evaluating crack/valley width and depth, are crucial for understanding crack healing mechanisms.

In our study, we introduce an innovative non-destructive, non-contact test method to evaluate the self-healing efficiency of cement-based materials with different healing agents. Following controlled damage, we conducted analyses using three-dimensional surface profiling to assess crack healing. This evaluation considered geometric and volumetric size variations in initiated micro-cracks and incorporated relevant surface roughness parameters for assessing self-healing performance at various time intervals.

2. Three-dimensional optical metrology system

Three-dimensional (3D) optical metrology represents the science of obtaining highly accurate measurements of an object's surface texture across three-dimensional axes. In contrast to conventional techniques like SEM, which may not provide accurate surface roughness and profiling information, 3D optical metrology offers distinct advantages.

3D optical metrological systems, which include methods like fringe projection, speckle metrology, and holographic interferometry, primarily rely on white light interference (WLI). These techniques have found widespread applications in fields such as biological recognition, reverse engineering, and industrial inspections. Their appeal lies in their ability to conduct rapid and precise measurements, making them invaluable tools for various industries and research endeavors [32]. In general, 3D metrology of an object is acquired through light wave interferometry. By combining and analyzing the resulting wave patterns, phases can be determined. This process allows for the extraction of information regarding the object's three-dimensional characteristics and surface features [33].

Fig. 1 shows a typical setup of a white light interferometer (WLI) with the light splitting and the associated reflection mechanism. The WLI operation mechanism works as follows; initially, light is emitted from a broadband light source such as incandescent lamps, halogen lamps, or, more recently, light emitting diode (LED) sources into the beam splitter [34]. Based on the designated ratio of the beam splitter, in general, the light beam is divided into two identical light beams where one of the beams is directed to a super-smooth reference mirror while the remaining light beam is directed to the surface of the sample. The lights from the reference mirror and surface object (i.e. tested light) are then reflected on the beam splitter and redirected to the main detector [35]. During the recombining process of the reflected light beam from the reference mirror and the tested light, black and bright bands are formed, called fringes, due to the interference between the two wavefronts (i.e., constructive interference phase). Fringes represent the topographical map and determine the surface roughness of the object as the result of the optical path difference (OPD) between the two wavefronts (Fig. 1) [36]. It can be noted, when the reflected light beams from the reference mirror and tested light are out-phase by 180°, then OPD is zero [37]. Subsequently, these fringes are continuously obtained during the scanning progress as a series of frames and received by the detector [38]. The theoretical signal interference signal at the detector can be represented by the following equations:

$$I(h, \Upsilon) = I_{DC} + I_{AC} \, cos[K(h - \Upsilon) + \Upsilon']$$

(3)

where I is interference Intensity, h is sample surface height or in position Υ of the object, Υ' phase offset and the I_{DC} and I_{AC} are constant
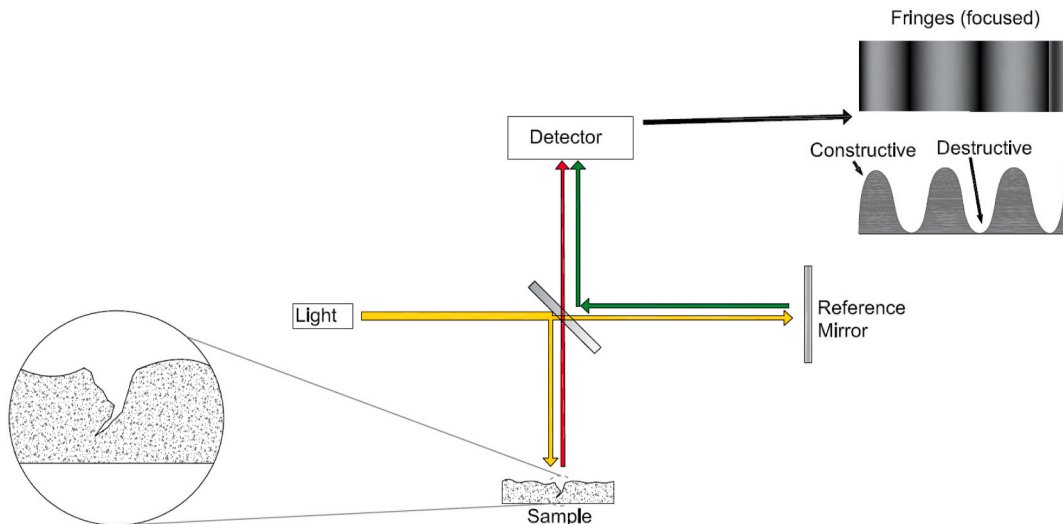

Fig. 1. Typical setup of White Light Interferometer for topological measurements.

values and

$$K = \left(\frac{4\pi}{\lambda}\right) cos(\Psi) \tag{4}$$

where λ is wavelength and Ψ is the angle between the illumination direction and the nominal scan or motion direction of the sample. K is known as the fringe's frequency. It correlates to the rate of the interference signals that oscillate sinusoidally at different sample's surface heights (h), (Υ) is the change in surface height in the position of the reference mirror and Υ' is the offset of the reference mirror [35].

By using different interferometric programs such as phase-shifting interferometry (PSI) for the surface roughness below 30 nm (Eqs. (3)–(13)) or vertical scanning interferometry (VSI) for surface roughness greater than 135 nm (Eq. (14)–(19)), the height is reconstructed point-by-point. Then, it is forwarded to the computer software, and a three-dimensional topography of the object is generated [39,40]. For the PSI technique, the digital process of obtaining the electronic images refines to [41].

$$\theta = Kh + \Upsilon' \tag{5}$$

Where θ is the starting phase offset (measured phase object).

In the conventional setup of the white light interferometry, as the object moves, the reference mirror is still stationary. Therefore, it can be assumed that the offset is constant and set at zero. Therefore, the equation for the surface height map is set to:

$$h = \theta/K \tag{6}$$

In the present type of white light interferometry, the object is stationary while the reference mirror is in motion. For such a scenario, the equation for the interference signals becomes:

$$I(\omega) = I_{DC} + I_{AC}\, cos(\theta + \psi) \tag{7}$$

Where,

$$\psi = -\,\Upsilon/4\pi \tag{8}$$

$I(\omega)$ is the interference signal and ψ is the phase shift in terms of the reference mirror for the Υ.

In general SPI operational systems, the reference mirror has linear communication with the phase shift (ψ) and for every image pixel, with the starting phase offset (θ) on the local surface height leads to intensity signal equation to:

$$I(\psi) = I_{DC} + I_{AC}[cos(\theta)cos(\psi) - sin(\theta)sin(\psi)] \tag{9}$$

To achieve the quadrature signals for the sine and cosine wave interference signals for the full cycle of the phase shift ψ, the following integrals can be drawn:

$$M = -\int_{-\pi}^{\pi} I(\psi)\sin(\psi)d\psi \tag{10}$$

$$N = -\int_{-\pi}^{\pi} I(\psi)\cos(\psi)d\psi \tag{11}$$

Therefore, phase θ is:

$$tan(\theta) = M/N \tag{12}$$

Relatively, the topological data acquisition as a result of the interference signals $I(\omega)$ is a sequence of digital captured camera frames at the detector, with a minimum of three to up to twenty intensity samples. Assume the acquisition of four sample intensities such as $I_{0,1,2,3}$ for the four-phase shift $\omega_{0,1,2,3}$, starting at $\omega_0 = -\frac{\pi}{3}$ and spaced at $\frac{\pi}{2}$ intervals, then, M and N become:

$$M = I_0 + I_1 - I_2 + I_3 \tag{13}$$

$$N = -I_0 + I_1 + I_2 - I_3 \tag{14}$$

Table 1
Phase shift interferometry algorithm with the phase shift and intensity sample quantity constant change.

$\Delta(\psi)$	Intensity samples	$tan(\theta)$
$\frac{\pi}{2}$	3	$\dfrac{I_0 - I_2}{-I_0 + 2I_1 - I_2}$
$\frac{\pi}{2}$	5	$\dfrac{2I_1 - 2I_3}{-I_0 + 2I_1 - I_4}$
$\frac{\pi}{2}$	7	$\dfrac{-I_0 + 7I_2 - 7I_4 + I_6}{-4I_0 + 8I_3 - 4I_5}$

The algorithm of phase-shifting interferometry for different intensity samples at a constant change of the phase shift $\Delta(\psi)$ is shown in Table 1.

Relatively, Vertical Shifting Interferometry is a typical technique used to measure the sample surface for engineering applications. Its advantage is determining the maximum fringe contrast along the vertical scanning direction. For the vertical scanning interferometry and obtaining electronic images, the process involves the rate of the interference fringes passed, as a function of the scan position over the surface sample where the frequency depends on the source wavelength λ. During the process of scanning the sample's surface on the angle of the incidence, the summed interference signals over a range of fringe frequencies are defined as [41]:

$$K(\beta, l) = 2l\beta \tag{15}$$

Where β and l are

$$\beta = \cos(\Phi) \tag{16}$$

and

$$l = 2\frac{\pi}{\lambda} \tag{17}$$

The factor of 2 represents the optical path change for a corresponding change in surface height, K represents the radian per micrometer, β is the directional cosine and l is the angular wavenumber for the spectral contribution.

The incident beam at angle ψ correlated to a specific image point and position at the pupil plane (i.e. for the Mirau interferometer, which operates in the same principles as the Michelson interferometer) the normalized contribution to the interference signals is:

$$Q(\beta, l, \Upsilon) = 1 + \cos\left(-K(\beta, l)\Upsilon + \Phi(\beta, l)\right) \tag{18}$$

Since the Mirau interferometer follows the same principles as the Michelson, then; Υ relates to the surface height (h), where:

$$\psi(\beta, l) = K(\beta, l)h + \partial(\beta, l) \tag{19}$$

The ∂ relates to the optical properties and the measured surface height:

Therefore, the conceptual mathematical superposition of all the angular wavenumber (l), all directional cosine (β) and the detection spectrum $V(l)$ the distribution for all image points at the pupil $U(\beta)$ is:

$$I(\Upsilon) = \int_0^\infty \int_0^1 Q(\beta, l, \Upsilon)U(\beta)V(l)\beta d\beta dl \tag{20}$$

The application of White Light Interferometry provides comprehensive measurements for engineering surface measurement [42]. One of the major limitations of the optical profilers is that only the topological information is achievable, while data angled beyond the surface of the sample is undetectable since the emitted light is non-bendable (Fig. 1).

3. Experimental program

3.1. Material and mix design

The ingredients used to prepare the concrete mixtures are general purpose cement (AS 3972) [43], sand (Haddens garden, Australia), and aggregate with nominal size of 7 mm and 10 mm (Mawsons, Australia). Microcapsules containing sodium silicate inside polyurethane shell material previously fabricated [44] and sodium silicate was obtained from local suppliers. Microcrystalline cellulose (MCC) (Avicel PH-101) powder (~100 % pure) received from FMC BioPolymer Corporation Inc was used as 'cellulose fibers' in this study.

Four concrete mixes were prepared with identical cement-sand and cement-water ratios of 0.54 and 1.85, respectively. Also, the aggregate contents (i.e. for 7 mm and 10 mm) were also identical for all three concrete mixes. Microcapsules at 5 % by the cement weight were added to one of the concrete mixtures, whereas 2.5 % cellulose fibers (by the weight of cement) were added to another concrete mixture. It can be noticed that the concrete mixes for control and direct method remain consistent (without the additional of healing agents), whereas samples from the direct mix was used to apply the healing agent directly (i.e. liquid sodium silicate) on the developed crack. The details of the concrete mix design and prospective healing agents are shown in Table 2.

Table 2
Concrete mix design for the various mixtures.

Concrete Mix	Cement (kg/m³)	Sand (kg/m³)	Aggregate 7 mm (kg/m³)	Aggregate 10 mm (kg/m³)	Water (kg/m³)	Microcapsules (kg/m³)	Cellulose Fiber (kg/m³)
Control	414.72	757.44	334.08	670.08	223.68	–	–
5 % MC	414.72	757.44	334.08	670.08	223.68	20.74	–
2.5%CF	414.72	757.44	334.08	670.08	223.68	–	10.38
Direct	414.72	757.44	334.08	670.08	223.68	–	–

3.2. Self-healing materials

In this study, self-healing materials consist of microcapsules that contain sodium silicate as the core material and polyurethane as the shell material. Microcapsules were fabricated and an average diametrical size of 100–200 μm was obtained (Fig. 2). Refer to Ref. [44] for more details on the fabrication process. Also, cellulose fibers were dispersed in water by overnight stirring and ultrasonication (for 15 min at 20 % amplitude, using QSonica 500 ultrasonicator) [45] and then mixed during the concrete mixing process. In addition, sodium silicate solution (30–60 % water suspension) was solely used by applying $0.1 \, \mu m^3$ (i.e., using a micro pipette) on the surfaces of the developed microcrack on the surface of the concrete sample.

3.3. Sample preparation

Concrete mixes were prepared in accordance with AS 1012.8.4 [46]. Initially, the dry components (i.e., cement, aggregates, and sand) were mixed in a small-scale mixer for 3 min; then, water was added, and the mixing progressed for an additional 3 min. Microcapsules were then added to the concrete mix that contained the healing agent and the mixing progressed for an additional minute. Alternatively, cellulose fibers were initially homogenized in the water required by the concrete mix and added to the dried mixture components, whilst mixing progressed for 3 min. Concrete cylindrical samples with a diametrical size of 40 mm and height of 80 mm were cast by using polyvinyl chloride pipes (i.e. ratio of 0.4:1 to the standard cylindrical concrete sample); later, the concrete samples were compacted by using a vibrating table at 50 Hz for 30 s. Concrete samples were then de-molded after 24 h and cured in wet conditions for 28 days.
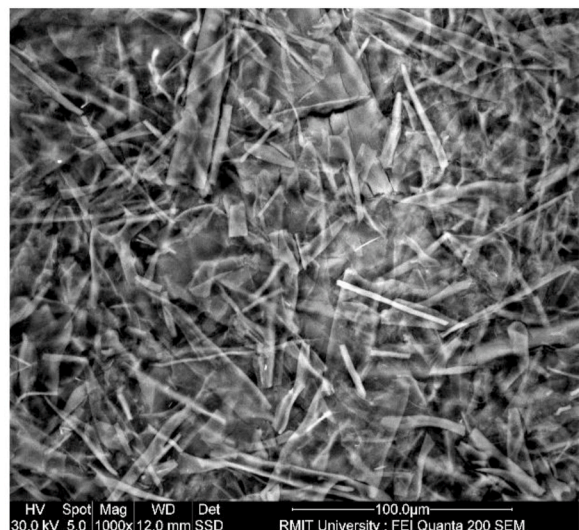
3.4. Crack development

After 28 days of curing, the concrete samples were dried at ambient temperature for 4 h. The experiment proceeded by testing the maximum compressive strength on a subset of samples. This value was then used to induce artificial cracks in the concrete specimens. Initially, unconfined maximum compressive strength from six replicates was obtained by applying an axial loading at 50 kN/min; the average unconfined maximum compressive strength was 13.78 ± 4.14 MPa, 14.7 ± 2.15 MPa and 13.0 ± 4.9 MPa for the control mix, 5%MS and 2.5%CF, respectively. Concrete specimens were then circumferentially confined with adhesive tape and positioned in the MTS-1000 machine. Localized micro-cracks were developed by applying 70 % of the unconfined maximum compressive strength for each of the concrete mixtures, respectively (Fig. 3). The damaged samples were cured under controlled conditions at a temperature of 24 Celsius and 80 % Relative Humidity and non-destructive non-contact tests were conducted after 0, 7, 14, and 28 days after controlled damage.

3.5. Surface morphology

Bruker Contour GTK-3D optical surface profiler was used to obtain the topological map of the concrete specimen surface and evaluate the crack healing performance and efficiency. Initially, the concrete specimen was placed on the stage of the microscope, then the specimen surface leveling was obtained to eliminate any slope-related concerns during the scanning progress. To enhance the reflectance light beam from the rough surface texture of the concrete specimen, the white light was replaced with green light and the optimum reflectance was achieved with 13 % light intensity. The incident light with the wavelength of 66.03 nm beam angled at 7.47°
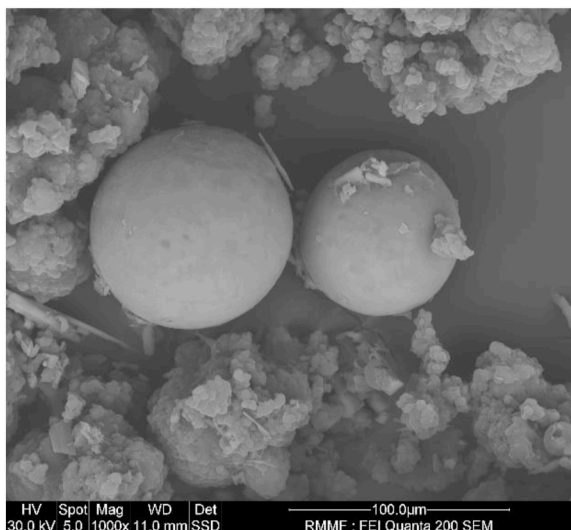
(A)   (B)

Fig. 2. SEM images (A) fabricated microcapsules (B) Cellulose fibers.

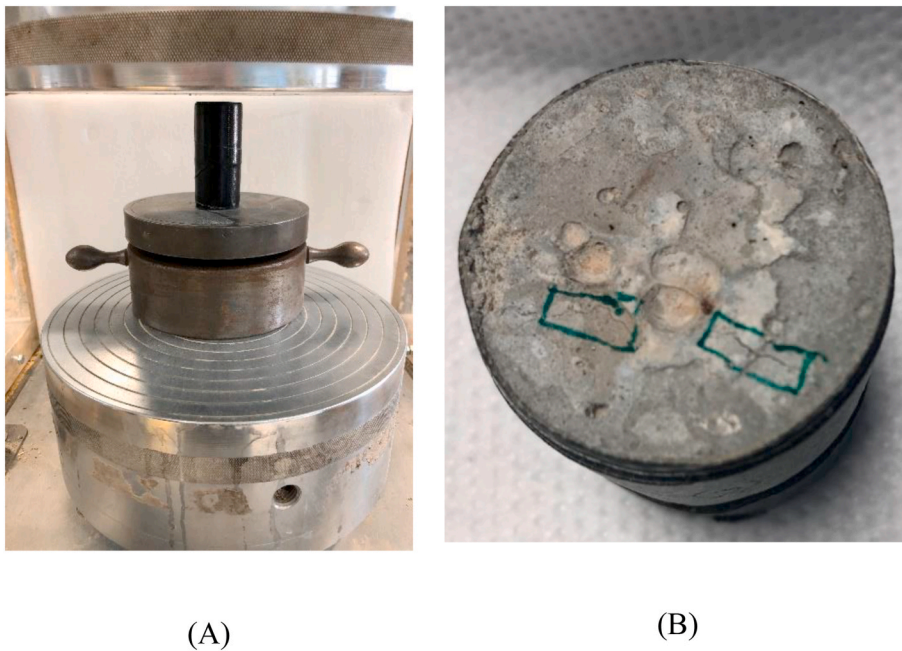(A)   (B)

Fig. 3. Crack development due to the axial-circumferential loading on concrete specimens (A) circumferentially confined with adhesive tape and (B) generated cracks on the surface of the specimen.
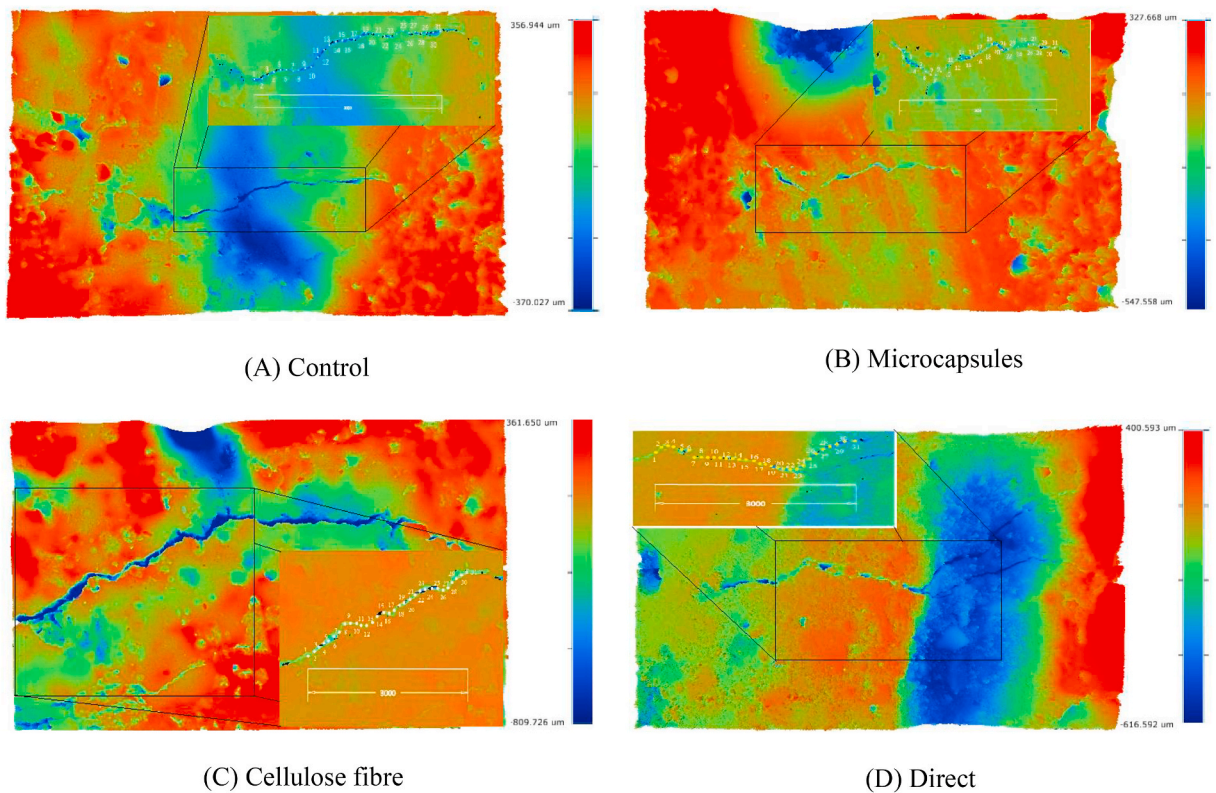

(A) Control   (B) Microcapsules

(C) Cellulose fibre   (D) Direct

Fig. 4. Tributary scan area and the selected points at approximately 100 μm intervals over 3000 μm in length and reference scale for height for different concrete mixtures (note: red color represents heights above the surface level of the concrete face and blue represents the depth below the surface level). (For interpretation of the references to color in this figure legend, the reader is referred to the Web version of this article.)

(i.e. NA = 0.13), which was sourced from the dual-LED illuminating lights. Vertical shifting interferometer (VSI) based on Michelson interferometry was selected to obtain a superior surface texture detection of the concrete specimen; since the surface texture is greater than 130 nm. The optical profiler was set to the depth detection of 950 μm and optimum segregation of the topological map was obtained at a threshold value of 3 % and a working distance of 6.7 mm (i.e. the distance between the specimen's surface and the front focal) hence, a topological map with a vertical resolution of 1.965 μm was obtained. Relatively, the scanning proceeded at the speed of 47 μm per second where a tributary scanning area in this study consists of 8×5 mm^2, hence self-healing efficiency was evaluated through the geometrical aspects, roughness, healing product volume and the angle of the cracks.

4. Results and discussion

In this experimental program, the concrete mixtures contained identical ratios of ingredients (i.e. sand, aggregates, cement, and water) but some were prepared by adding 5 % microcapsules or 2.5 % cellulose fibers, respectively. During the sample preparation, some trends were visually recognized such as the loss of plasticity, typically for the concrete mixture containing the microcapsules, which can be attributed to the water absorption of the polyurethane material mixed in the cementitious matrix. Whilst minimal effect on the loss of plasticity was recognized for the concrete mixture containing cellulose fibers in comparison to the control concrete mixture. After 28 days of curing, due to the healing agent additives mixed in the concrete mixtures leading to partially reduce the effective water content available in the concrete mixtures, the density for the control, cellulose fibers and microcapsules concrete mixtures were 2313.45 ± 11.21 kg/m^3, 2291.44 ± 11.24 kg/m^3 and 2236.88 ± 6.51 kg/m^3, respectively. Seemingly, the additional 5 % microcapsules content and 2.5 % cellulose fibers have reduced the density by 3.3 % and 0.95 %, respectively, in comparison to the control mixture. This indicates that the addition of the healing agent potentially reduces the mechanical properties of the concrete material. Such a reduction was expected at the initial stages of the experiment as a result of the incremental ratio of the powder to water content in the cementitious matrix. Moreover, a 3D surface morphology test was conducted with the tributary scanning area of 5 $\times$ 8 mm for the different concrete mixtures. To ensure the same crack is scanned throughout the experimental program, approximately,

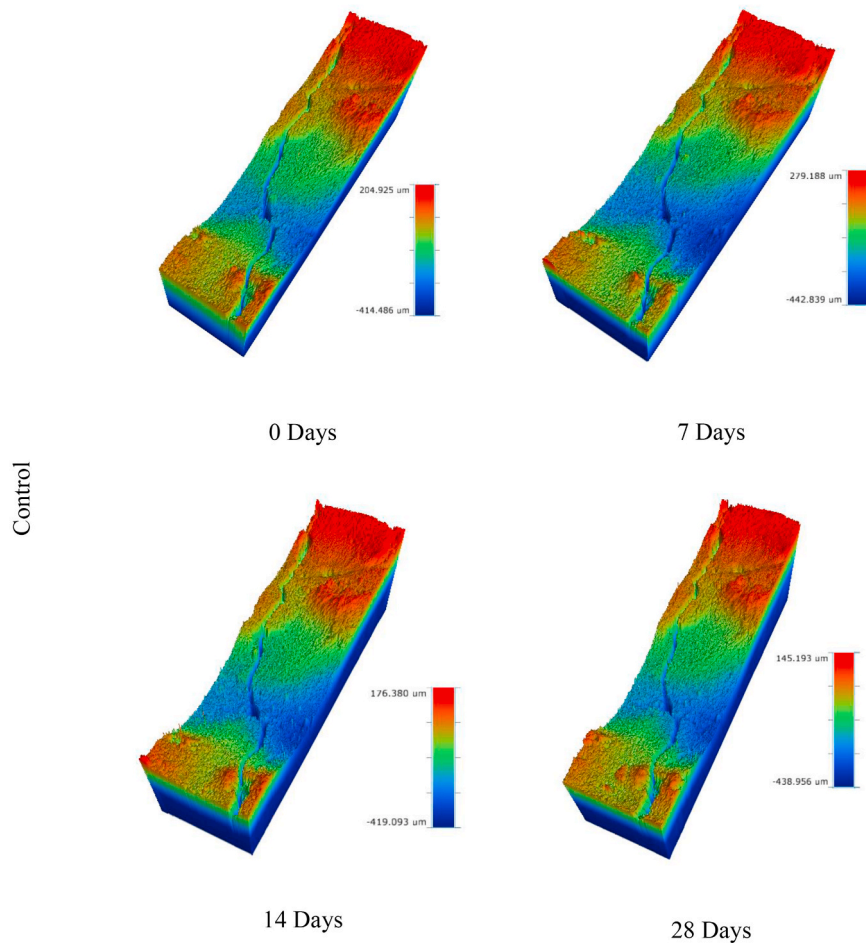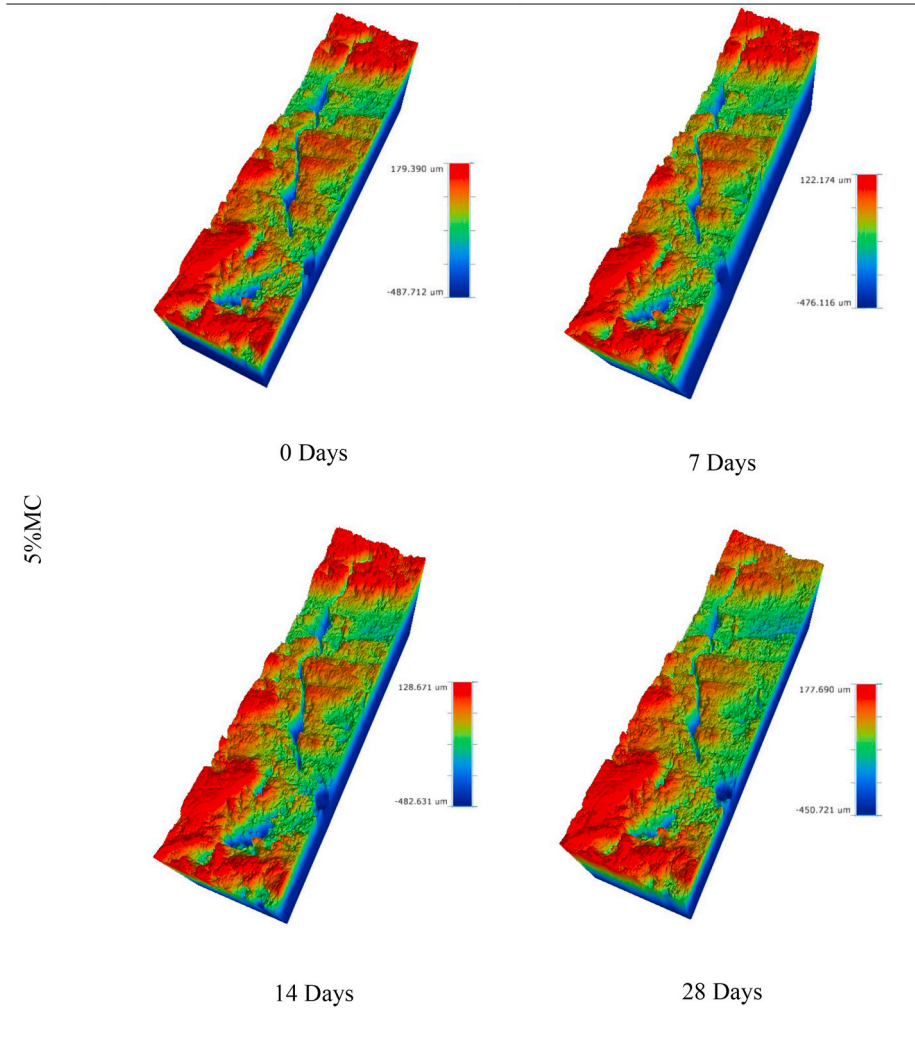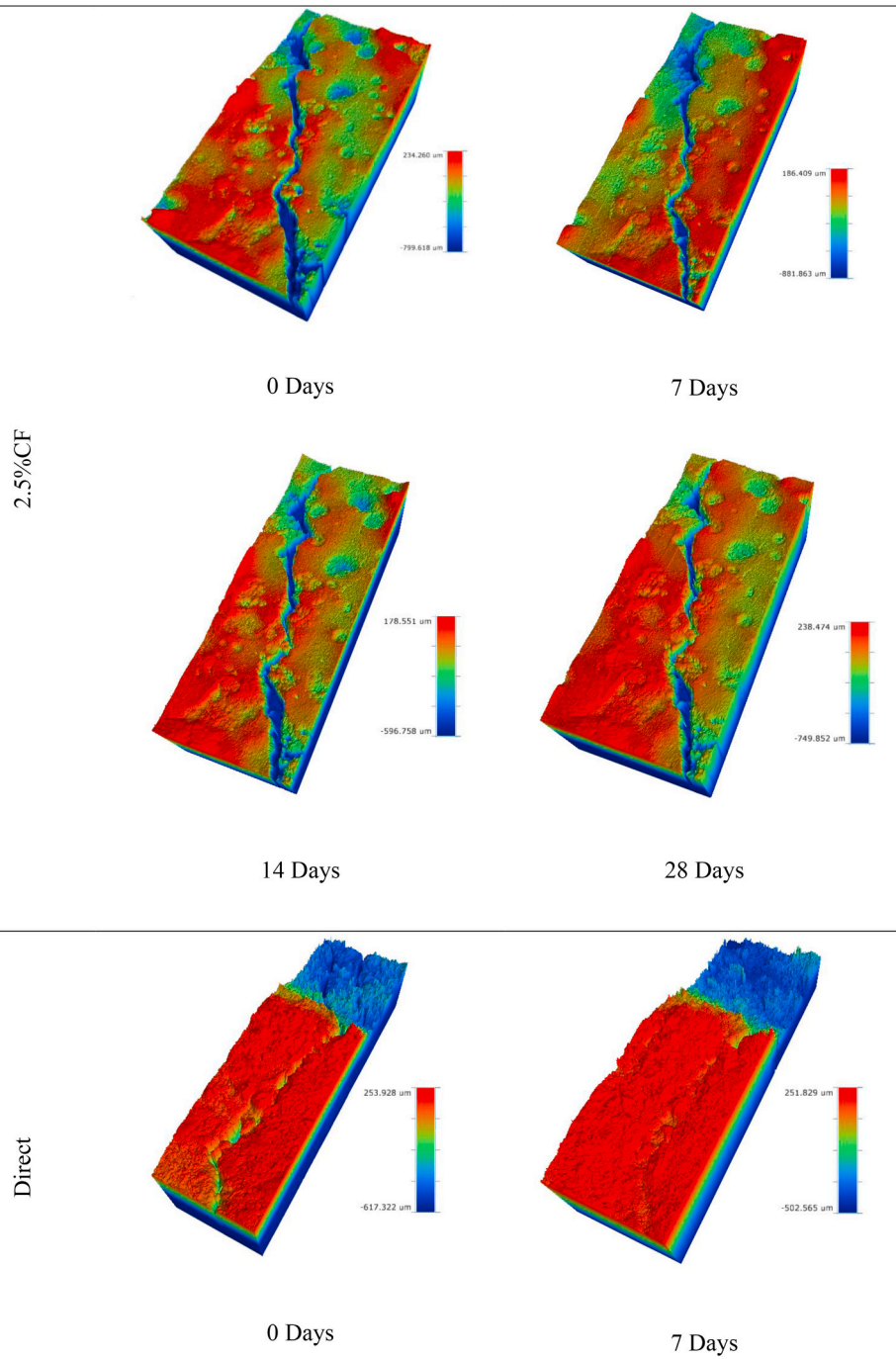**Fig. 5.** Surface morphology for the different concrete mixtures at various time intervals.

0 Days

7 Days

5%MC

14 Days

28 Days

Fig. 5. (*continued*).

2.5%CF

0 Days

7 Days

14 Days

28 Days

Direct

0 Days

7 Days

Fig. 5. (*continued*).
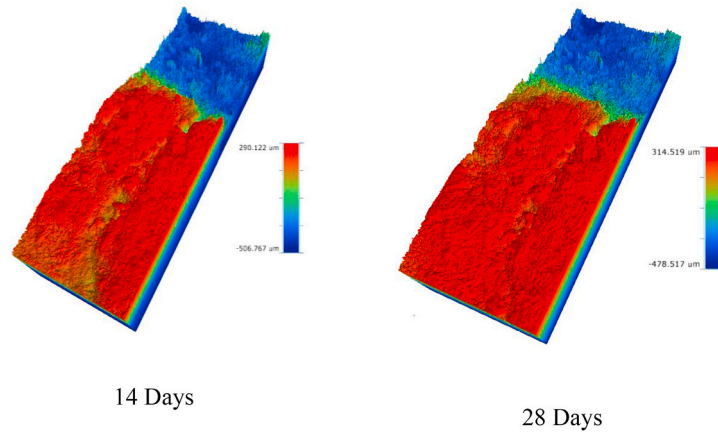
14 Days

28 Days

Fig. 5. (*continued*).

the same coordinates were scanned at different time intervals (i.e., after 0, 7, 14, and 28 days post-curing). Relatively, analysis of the crack/valley width, depth and contact angle coupled with the healing product content were determined throughout the experimental program at 100 μm intervals over 3000 μm length in the direction of the x-axis, as shown in Fig. 4.

4.1. Optical assessment

Visual testing techniques were initially used to directly observe the changes that occurred during the healing progress due to the different healing agents. A control concrete specimen is also used to calibrate the autogenous and autonomous healing performance in the cementitious materials. The surface morphology testing technique shows the morphological information of the damaged region and the location of the formed microcrack on the surface of the concrete specimen. Also, due to the vibration mechanism during the sample preparation leading to partial relocation of the aggregates to the lower levels and uplifting of the cementitious materials toward the top of the specimen, crack formation occurred in the cementitious materials, rather than at the Interfacial Transition Zone or the fracture of the aggregates itself, since fine aggregates can be visible when the optical resolution is increased [47]. Fig. 5 shows the surface morphology of the cracks and variation in the valleys (i.e. depth and width) due to the healing process as a result of the healing agent materials. The crack depth in the figure is linked with negative values (i.e. closer to the blue color) while the topological areas relate to the positive values (i.e. closer to the red color). Seemingly, the control specimen showed minimum healing from the autogenous healing mechanism and only a fraction of the crack was healed after 28 days of post-curing. It can be attributed that the healing progress was minimal through the autogenous mechanism; alternatively, the healing volume is drastically low and cannot be observed visually toward the end of the experiment. Effectively, the concrete mixture 5%MC has two segments of the crack with a
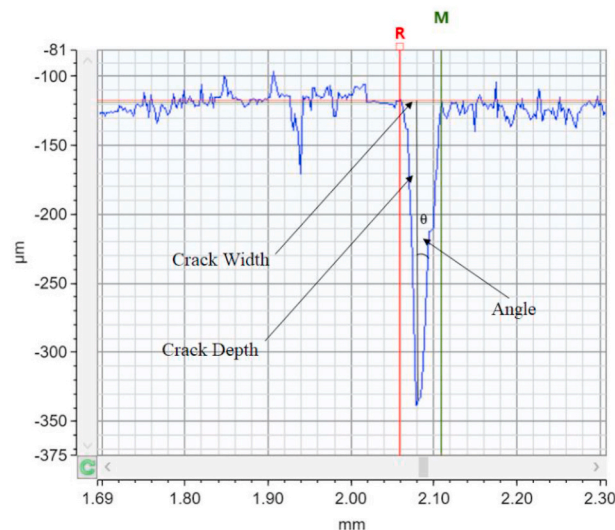

Fig. 6. Systematic methodology of obtaining the crack geometry for selected points of each concrete mixture.

(A) Control

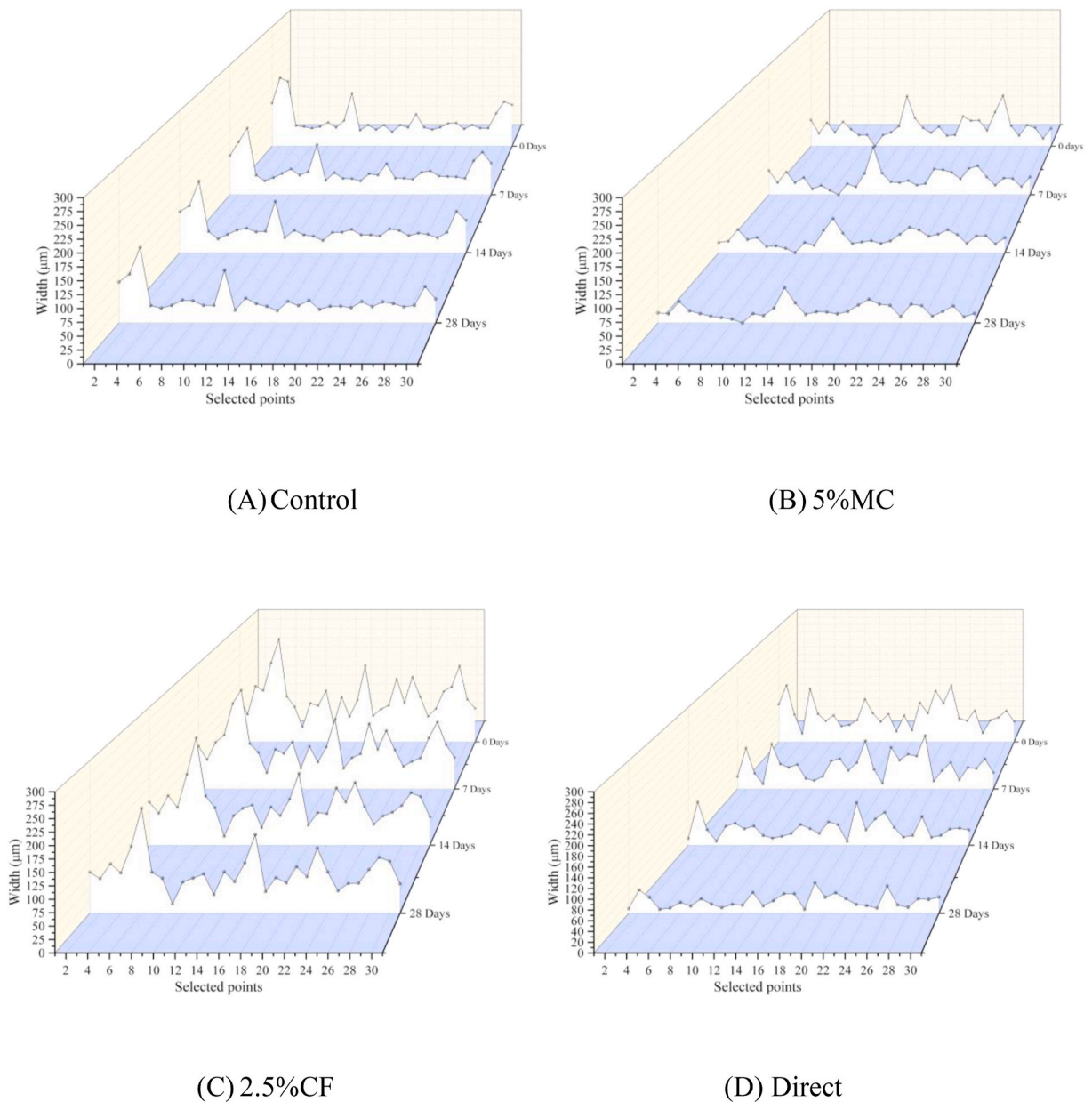(B) 5%MC

(C) 2.5%CF

(D) Direct

Fig. 7. Crack width for different concrete mixtures for each of the selected points during the healing progress.

rougher surface in comparison to the control specimen. The crack healing was not achieved from the early stages of the crack development (i.e. from 0 days to 14 days), although, it was more evident from 14 to 28 days of post-curing (Fig. 5_5%MC), as segments of the crack were healed and resulted in closing the crack width. This can be attributed to the chemical reaction between the sodium silicate and the calcium hydroxide particle, thus leading to the formation of the newly formed CSH materials (see Eqs. (1) and (2)) after 14 days from the microcapsules breakage. Similar results were reported by Sidiq et al. [48]; in this case, the authors showed the recovery of the mechanical properties was obtained after 14–28 days of breaking the microcapsules in the cementitious matrix. Furthermore, the healing progress for the concrete mixture with a 2.5 % cellulose fiber content was not initially significant during the early stages of microcrack development. However, after 28 days of crack development, some healing was observed, particularly in the section with the smallest crack width (Fig. 5_2.5%CF). Thus revealing how the addition of cellulose fibers in cementitious materials can be effective in promoting self-healing. Similarly, in a study conducted by Harshbab and Gupta [49], crack healing was obtained after 21 days of post-crack development with a recovery of 48.7 % by using cellulose fibers as the healing agent. The analysis conducted via Ultrasonic Velocity Pulse showed 7.84 % regain in flexural strength in comparison to the control mixture. Furthermore, the condition of the self-healing was accelerated by applying sodium silicate directly on the cross-sectional area of the formed microcrack, thus, the

healing product was obtained after 7 days of the crack development, while the healing product incremented after 14 days and the full recovery was obtained after 28 days (i.e., after 28 days post curing). Notably, the identical sodium silicate solution that has been encapsulated inside the polyurethane materials, had a lesser effect on self-healing progress in comparison to applying sodium silicate directly on the cracked section. This mechanism can be due to the presence of a greater quantity of sodium silicate on the crack segment, thus leading to a greater content of sodium silicate molecules reacting with unhydrated calcium.

4.2. Crack closure

Crack closure variation is assessed through the crack width and depth across the length of the formed crack as shown in Fig. 4. In this section, the crack width is measured at the surface of the specimen as the distance existing between the two crack walls perpendicular to the crack's path. The crack depth is measured at the same location where the crack width is measured as the vertical distance toward the lowest detected location of the crack opening (i.e. bottom of the valley). Note that the measured depth is perpendicular to the crack width but not necessarily in the middle of the crack width since the valley formation might not be symmetrical. Fig. 6 shows the systematic morphology of obtaining the crack width and depth measurements for individual points (Fig. 4).

Fig. 7 shows the progress of the crack healing based on the crack width assessment at different time intervals for the four concrete mixtures. Seemingly for the control mixture, at the initial stages of the autogenous healing progress, the crack width ranges from 35.4 μm to 171.6 μm through the crack length. The effectiveness of crack healing in higher crack width ranges for the control sample is
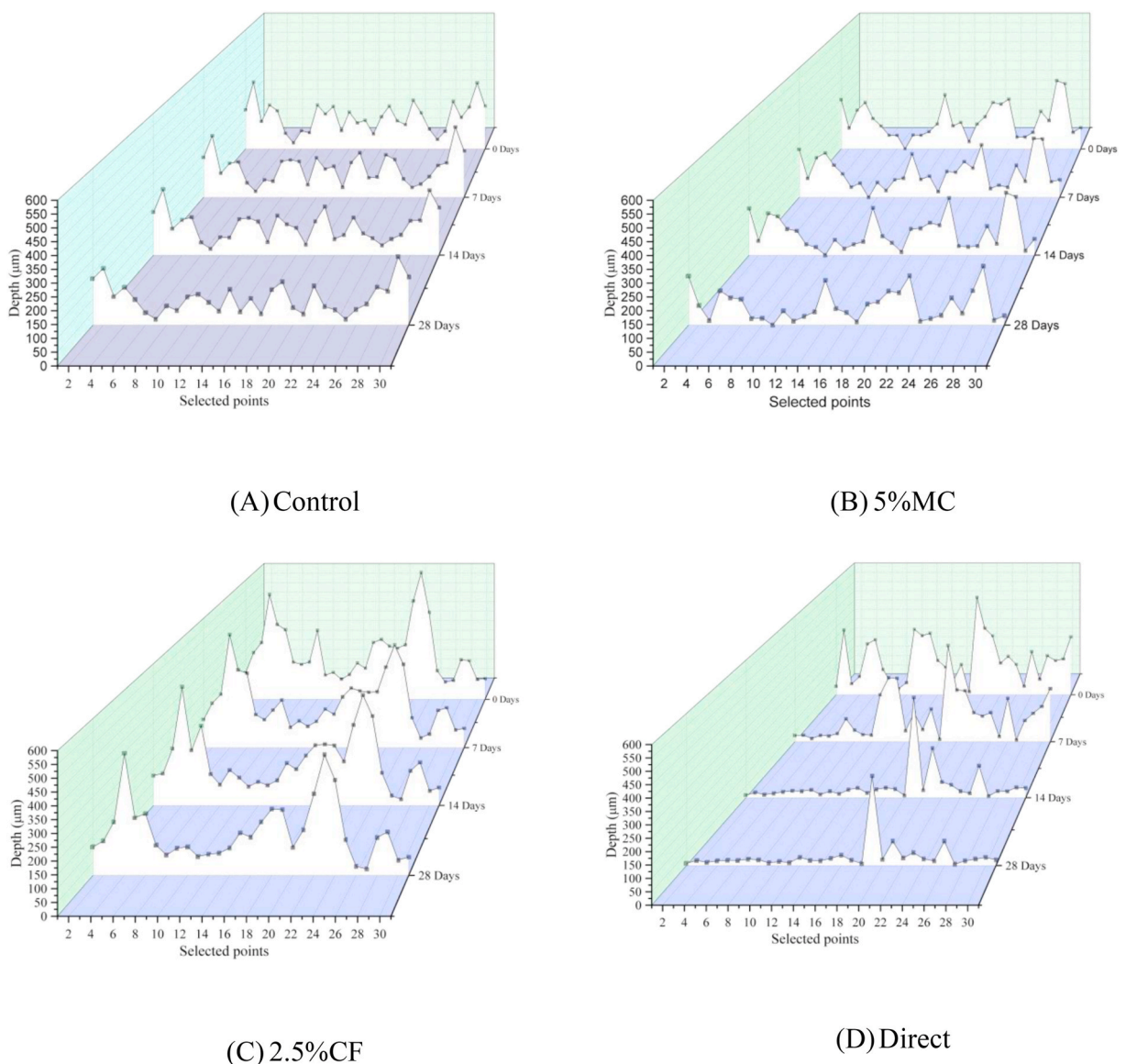

(A) Control

(B) 5%MC

(C) 2.5%CF

(D) Direct

Fig. 8. Crack depth of each of the selected points for different concrete mixtures during the healing progress.
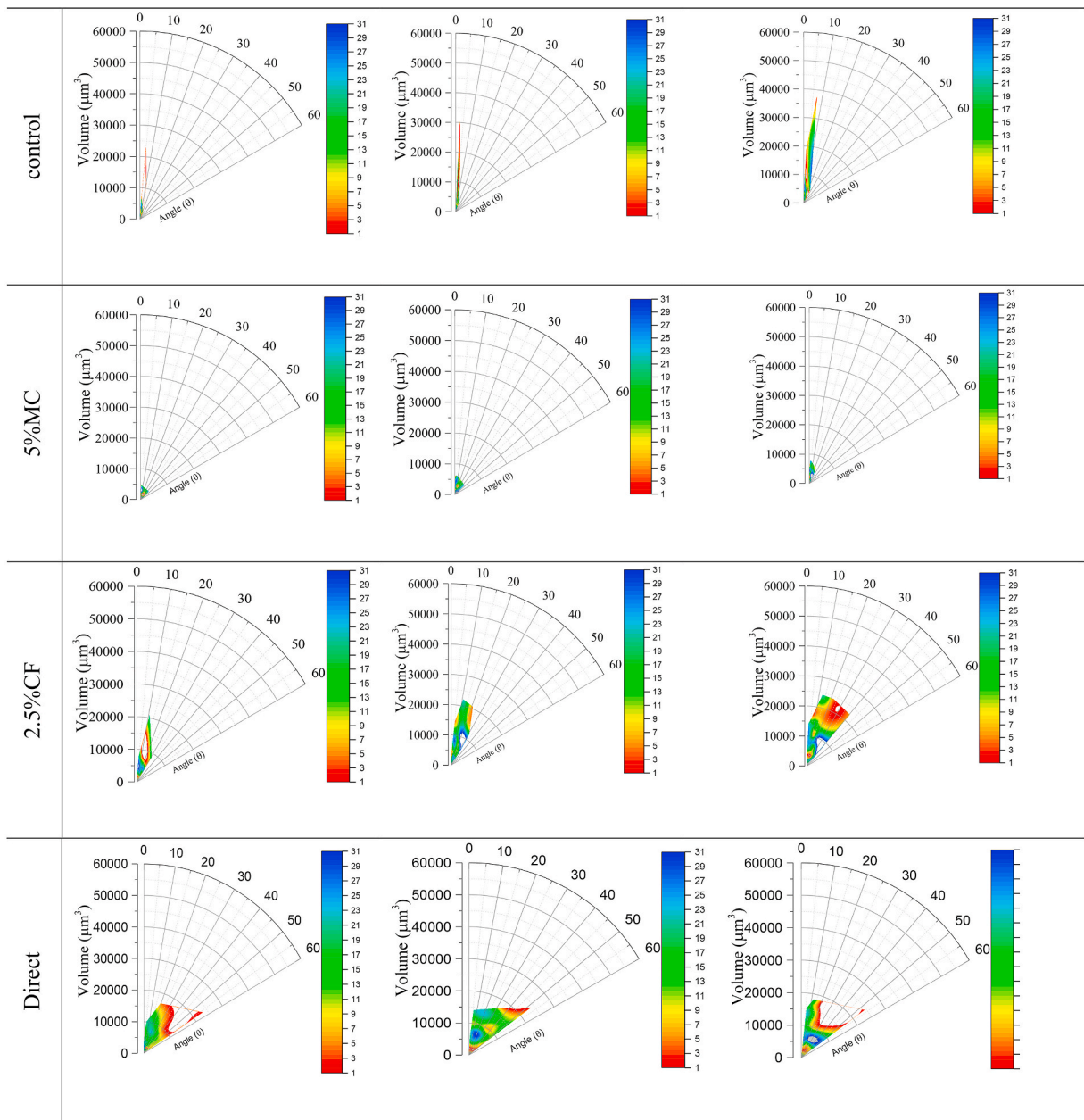
Fig. 9. Tangential angle for each of the selected points for different concrete mixtures at different times of healing progress (i.e. from the right side of the crack).

minimum and more self-healing occurs for the crack width in the lower ranges of aperture. Comparably, the concrete mixture 5%MC showed crack widths of up to 127.5 μm, however, as a result of the microcapsule rupture during the crack formation mechanism and the formation of the C–S–H gel, the crack healing in most of the points throughout the crack length progressed effectively. For instance, after 14 days from the crack formation, the crack width was reduced by 42.6 % and 54.9 % at points 13 and 24, respectively. Furthermore, after 28 days, the crack width closure for the same points (i.e. points 13 and 24) was approximately 46.5 % and 86.1 %, respectively. Indicating the self-healing is likely occurring in the crack walls. Moreover, the crack width for the concrete mixture 2.5% CF ranges from 39 μm to 276.2 μm, which is effectively greater than the other concrete mixtures. It was observed that the crack width closure performance due to the addition of the cellulose fibers is negligible until 14 days of the post-crack formation and instead occurs after 28 days. This can be attributed to the fibers acting as the bridging element in the cementitious matrix. Similar results were found by Bentchikou et al. [50]; the authors evaluated the flexural strength of the concrete mixture with various cellulose contents and found

that the flexural strength increased after damage at cellulose content greater than 4 %, while it reduced at fiber content below 4 %.

Lastly, for the concrete mixture that followed the direct application of the sodium silicate solution, the crack width ranged from 21.7 μm to 147.6 μm. Seemingly, the healing progress for the crack width closure is drastically greater in comparison to the remaining concrete mixtures, as the result of its direct application. Hence the crack is filled with a healing agent.

The healing performance was assessed based on the crack depth. Fig. 8 shows the crack depth healing progress for all of the concrete mixtures at different time intervals. For the control mixture, the crack depth ranged from 30.3 μm to 336.9 μm, however, as a result of the autogenous healing mechanism, the depth slightly changed toward the lower values of the interval. After 7 days, the crack depth range was reduced by 3.2–7.5 % in comparison to the original crack depth (i.e. 30.3 μm–336.9 μm). After 28 days of healing, the crack depth is reduced by 22.3–34.1 %. It was observed that self-healing is more evident when the depth of the crack is smaller. As the crack walls are becoming narrower, the crack depth is also reduced due to autogenous healing. Indicating, autogenous self-healing is greatly dependent on the distance between the crack walls. The concrete mixture 5%MC showed a consistent self-healing mechanism over time. The addition of the microcapsules led to the autonomous healing mechanism in combination with the autogenous process to produce an effect on healing cracks when the crack walls are closer to each other (i.e. crack walls are generally closer at the bottom of the valley compared to the top section of the valley). Similarly, for the concrete mixture 2.5%CF, the healing performance is also dependent on the initial crack width and healing time since the crack depth is reduced progressively at different time intervals. In this case, the range of the crack depth initially varies between 87.6 μm and 639.7 μm. After 14 days, the range is reduced by 21.5–69.7 % and, after 28 days, by 26.9–71.4 %, which is almost double in comparison to the control concrete mixture. As already postulated, cellulose fibers are thought to be more effective in joining the crack walls when they are closer to each other [51]. Lastly, the direct
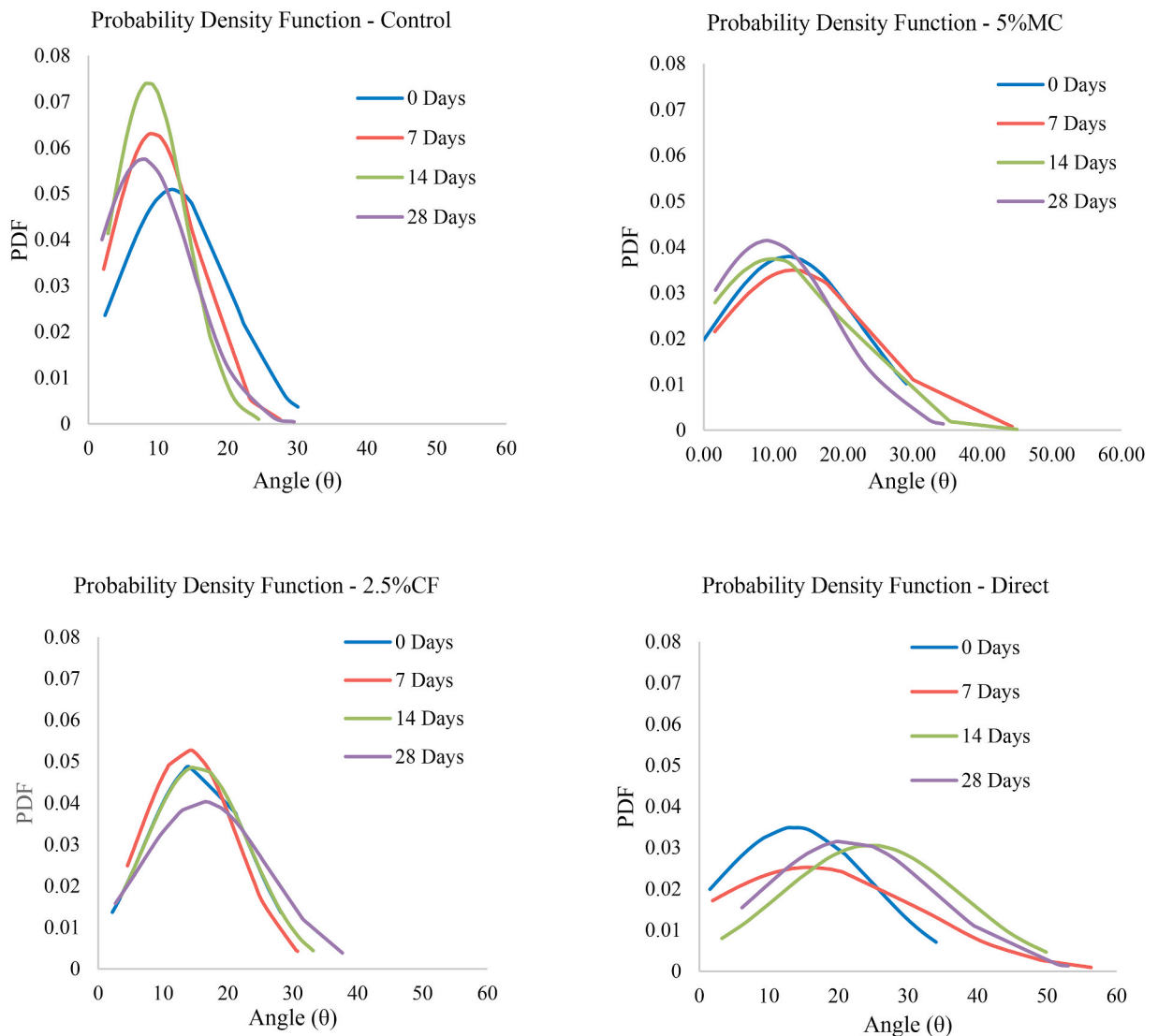

Fig. 10. Probability Density Function for crack angles for different concrete mixtures during the healing progress.

application of the sodium silicate produced the best results due to the solution penetrating inside the crack, hence acting as a filling agent (Fig. 8D).

4.3. Assessment of the healed volume via contact angle analysis

Further to the crack depth and width, crack healing through the volumetric size was determined at different time intervals at 100 μm thickness across the crack length then subtracting from the initial volume at 0 days post curing (i.e. right after the cracking occurrence). Then, the healing performance was also evaluated based on the healing product content and the angle of the healing product. The angles were obtained from the adjacent crack depth to the farthest crack wall as shown in Fig. 6. The rationale for this type of analysis is to evaluate the crack healing progress as the results of the geometrical variation of the crack during the crack healing from the crack depth and crack width. The healing product and associated angle for each of the concrete mixture are shown in Fig. 9. For the control mixture, the healing product is relatively low at 7 days and it is spread at various angles ranging from 0 to 20°, indicating crack healing performance is more likely occurring through the narrow crack width. After 14 days, the healing content increased with the corresponding angle shifting toward lower angles, which indicates the crack width is becoming narrower and therefore smaller angle values are observed. As a result of the autogenous healing mechanism in the cementitious matrix, after 28 days of crack formation, the healing volume is increasing, and the angles are shifting toward larger values. Healing occurred from the lower regions of the crack, hence leading to larger angles. It can be explained that crack healing was more pronounced along the crack wall due to the larger surface area exposed to environmental conditions. Consequently, this led to a greater occurrence of autogenous self-healing, resulting in the narrowing of the crack. The distance between the two crack walls is shortened resulting in greater healing progress from the lower region. A similar observation was obtained in the crack width and depth analysis section. For the concrete mixture 5%MC, healing was coupled with very low angles ranging between 0 and 50° (i.e. after 7 days). However, the healing product is almost doubled in comparison to the control specimen due to the release of sodium silicate during the capsule breaking process and consequent formation of the C–S–H gel. Furthermore, healing progressed at 14 days at almost similar angle ranges, showing that healing was accruing from the lower regions of the crack and crack walls. After 28 days, crack healing occurred at the crack walls since the angle values are shifted toward lower ranges.

For the concrete mixture 2.5%CF, the angles associated to self-healing ranged between 0 and 30° (i.e. after 7 days), indicating the crack healing is occurring in the narrow crack width and the healed product is approximately doubled in comparison to the control mixture and at the same time interval. The self-healing performance remains in the same angle ranges (i.e. 0-30°) after 14 days, while the healing product increases, indicating the crack healing is occurring in the narrow crack width rather than the crack depth. This indicates that the crack walls become closer to each other, and it can be attributed to the combination of the autogenous self-healing (i. e. due to the greater surface area of the crack walls) and the additions of the cellulose fibers acting as physical links to promote crack closure. However, after 28 days, the self-healing performance becomes greater and the angle increases to 0–40° which indicates the crack healing occurred from the depth of the crack, thus leading to wider crack's angle. Such healing mechanism indicates that at initial time intervals crack self-healing is easier to achieve at the crack walls and, as the crack becomes narrower, crack healing initiates from the depth of the crack. For the concrete mixture where sodium silicate was directly applied on the initiated crack, the self-healing performance is occurring at angle ranges of 0–50° and the healing product (i.e. after 7 days) is approximately four times that of the control sample. The healing performance is more evident for narrower angles (i.e. crack walls rather than in the crack depth), thus the healing product is more shifted toward the lower angles. An explanation for such narrowing of the angle can be due to the greater surface area of the crack wall and the intaking of greater content of the sodium silicate solution leading to greater self-healing performance. The self-healing was further progressed after 14 days as the healing occurred at larger angles (i.e. greater healing content is towards the larger angles). The healing mechanism indicates that healing is more present in the crack depth at this time interval. After 28 days, the crack healing was obtained at lower angles. The healing agent (i.e. sodium silicate) directly promotes self-healing initially within the crack wall, then healing is progressed in the crack depth and then shifted to the crack walls to fully fill the unhydrated C–H–S product.

Moreover, statistical analyses have been conducted to evaluate the variation of the crack healing at different angles and different time intervals. In order to characterize the density of the angles for all different concrete mixtures during the healing progress, the Probability Density Function (PDF) has been used by using Eq. (21) [52]. Fig. 10 shows the probability density function for the different angles obtained for all different concrete mixtures at various time intervals. For the control sample, the average angle after the crack development is $12.10° \pm 11.46$ (i.e. 0 days of curing) and positively skewed, indicating the crack contains angles of more than the average value. After 7 days, the peak is shifted toward the left with an average angle of $9.28° \pm 6.31$, indicating the crack healing performance occurred in the crack walls compared to the crack depth, similar results were observed in the crack width and depth section. After 14 the healing performance of the healing is slightly increased and the average angle is $8.64° \pm 5.38$ and higher PDF values indicate healing progress is increasing, while after 28 days the average angle is changed to $7.85° \pm 9.64$. The mechanism of the crack healing clearly shows that self-healing is occurring within the crack wall and at 28 days the healing is more occurring at the depth of the crack (i.e. lower value of PDF). For the concrete mixture 5%MC the average angle is $12.03° \pm 14.64$ (i.e. 0 days) and positively skewed which shows most of the cracks are larger than the average value. After 7 days the average angle is almost similar (i. e. compared to 0 days), it can be noticed that in the previous section healing product was obtained while the angle is similar to the initial crack development and this can be explained by that the healing performance was occurring within the crack walls and depth subsequently leading the angle changing limited. After 14 days, the average angle is $9.49° \pm 10.63$ which is and increased PDF value indicating healing progress is in the crack walls. Similar results were observed by A.Sidiq. et al. [48] as the authors' microcapsules contained sodium silicate as the healing agent encapsulated in polyurethane shell materials and assessed self-healing performance by the mean of the mechanical and non-destructive test methods (i.e. x-ray tomography) and healing was achieved after 14 days of crack

development. Subsequently, after 28 days the average angle is further reduced to 8.88° ± 9.63 which shows further healing performance within the crack walls and depth (i.e. average angle is near for the 14 days and 28 days). Moreover, for the concrete mixture 2.5%CF, the average angle is 14.88° ± 8.44 (i.e. 0 days) and after 7 days the average angle is changed to 13.33° ± 7.84 indicating a slight healing performance within crack walls and potentially the healing performance progress is in the crack depth. The average angle after 14 days and 28 days is increased to 14.71° ± 8.49 and 15.67° ± 10.15, respectively, indicating the crack healing is more likely occurring within the depth of the crack in comparison to the crack walls. For the concrete mixture where sodium silicate (healing agent) was applied directly on the crack, the average angle is 13.64° ± 11.44 and positively skewed, indicating that most of the cracks were greater than the average value. The average angle is increased to 15.81° ± 15.80 and 24.61° ± 13.03 for 7 days and 14 days, respectively, indicating the healing performance was more progressive at the crack depth. However, the average angle reduces to 21.23° ± 12.60 at 28 days which illustrates the crack becomes narrower indicating the crack healing is within the crack wall. Similar results have been observed in earlier sections.
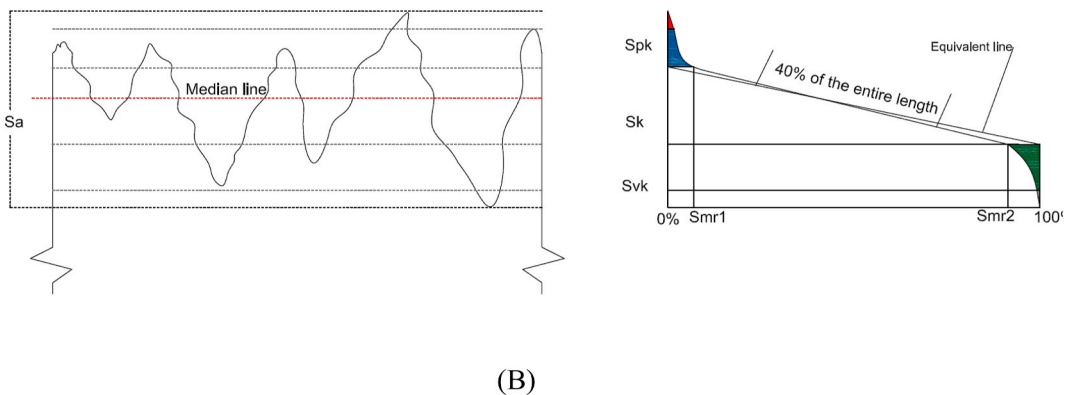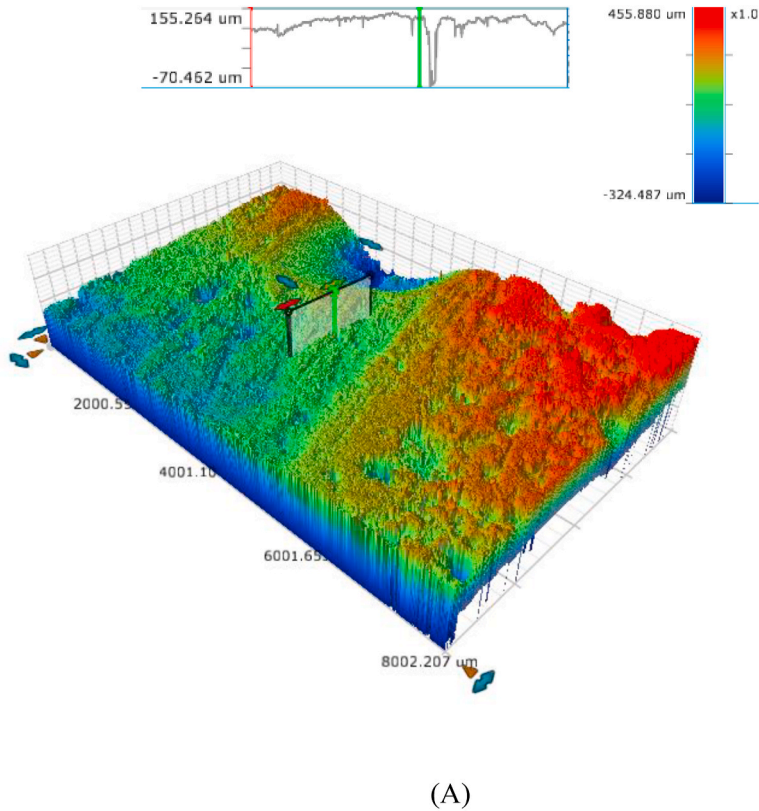

(A)

(B)

Fig. 11. Systematic plan of the surface roughness measurement (A) surface texture of the concrete specimen and the identified valley (B) surface roughness parameters identification.
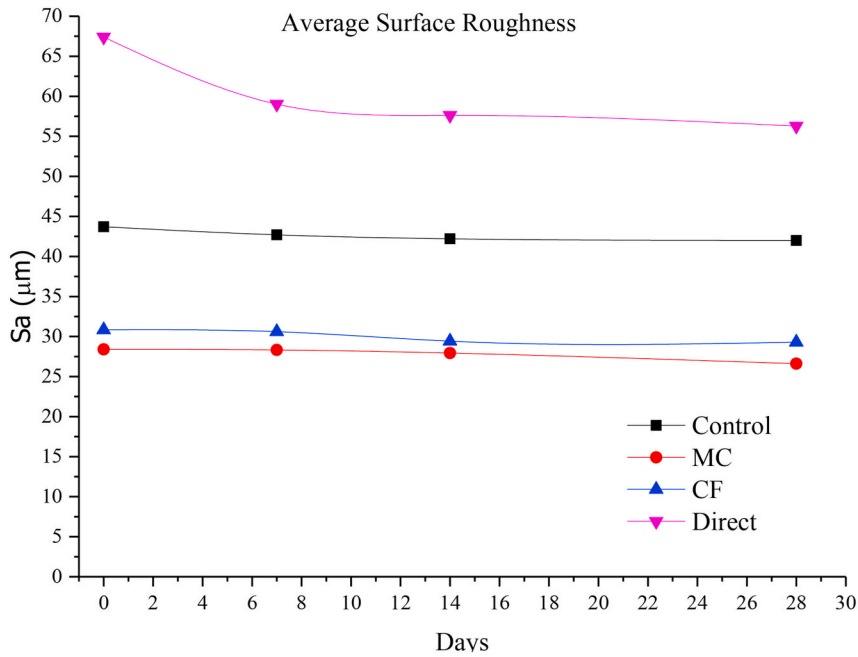
Fig. 12. Arithmetical mean height – Sa-value for different concrete mixtures.

$$f(x) = \frac{1}{\sigma(2\pi)^{\frac{1}{2}}} exp\left[-\frac{(x-\mu)^2}{2\sigma^2} \right] \tag{21}$$

Where, x, σ and μ represent the angle data variable and standard deviation, respectively [52].

4.4. Morphological parameters approach

There are a number of surface texture parameters identified by ISO 25178 [53] to assess the surface roughness for different engineering disciplines. These parameters are obtained based on the reference surface for a measured area and specifying the heights throughout the measured area and calculating the deviation of the heights when the reference surface (i.e. height) is zero [54]. These parameters are categorized based on their functionality and for this study, typical parameters are selected (i.e. from a range of parameters) which are most applicable for the self-healing evaluation in relation to the variation in surface roughness, specifically, for the crack valley and volumetric size. Thus, arithmetic mean height and root mean square height (height parameters category), valley material portion (functional parameters category) and dale void volume (volume parameters category) are selected. Fig. 11 illustrates the different surface roughness parameters used in this study in relation to the peak and valley on the surface of the concrete specimens.

4.4.1. Arithmetical mean height (Sa-value)

Arithmetical mean height is defined as the difference in height for the area of interest compared to the arithmetical mean value (Eq. (22)) [54], which supports evaluating the crack depth and the healing performance evaluation during the different time intervals. Fig. 12 illustrates the arithmetical mean height (Sa-value) during the healing progress for the different concrete mixtures, respectively with time. The Sa-value decreased during the healing time intervals for all concrete mixtures, sloping downward toward the right direction, indicating crack depth is becoming shallower with time. Thus, for the control mixture, the Sa-value is reduced by approximately 3.4 % till 14 days due to the autogenous self-healing, while the Sa-value nearly remained unchanged at 28 days highlighting lower healing performance. For the concrete mixture 2.5%CF, the Sa-value is reduced by approximately 4.6 % till 14 days and at 28 days the Sa-value is slightly reduced. It can be noticed that the addition of the cellulose fibers has been effective in reducing the crack depth further by 35.6 % in comparison to the control mixture at 14 days. Similar results were obtained from crack depth in the earlier section since the Sa-value is relative to the peak and valley of the surface. Furthermore, for the concrete mixture 5%MC, the Sa-value is low till 14 days and it is reduced by approximately 1.6 % while at 28 days the Sa-value is further reduced to approximately 4.7 % (i.e. total Sa-value reduction of 6.3 %). It can be noticed that for the concrete mixture containing the microcapsules the self-healing performance significantly increased from 14 days to 28 days which can be attributed that the chemical reaction between the newly formed cementitious product (i.e. due to the chemical reaction from sodium silicate and calcium) at the bottom of the crack is hardened during such time interval. Similar observations are obtained from the authors' previous study [48], which assessed the self-healing performance through mechanical and non-destructive tests methods. For the concrete specimen where the sodium silicate solution was directly applied on the initiated crack, the Sa-value is reduced significantly by 12.2 % at 7 days and a further Sa-value
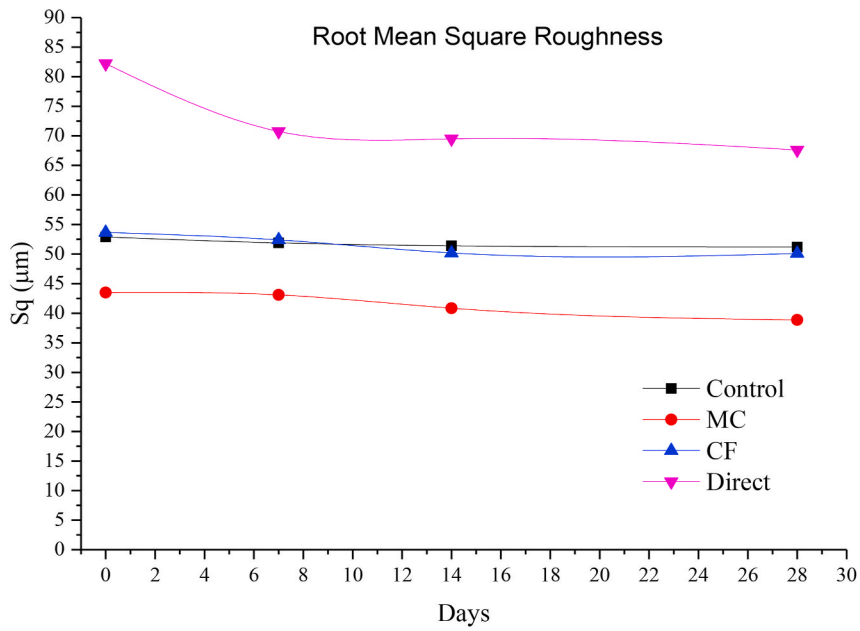
Fig. 13. Root Mean Square Height (Sq-Value) for different concrete mixtures.

reduction of 2.33 % and 16.5 % was observed at 14 days and at 28 days, respectively. Notably, the direct application of healing agents on the surface of developed cracks has the potential for self-healing at a high performance level.

$$Sa = \frac{1}{A}\iint_A |Z(x,y)|dxdy \qquad (22)$$

Where Sa is the Arithmetical mean height, A is the surface area and x, y, z are the cartesian coordinates.
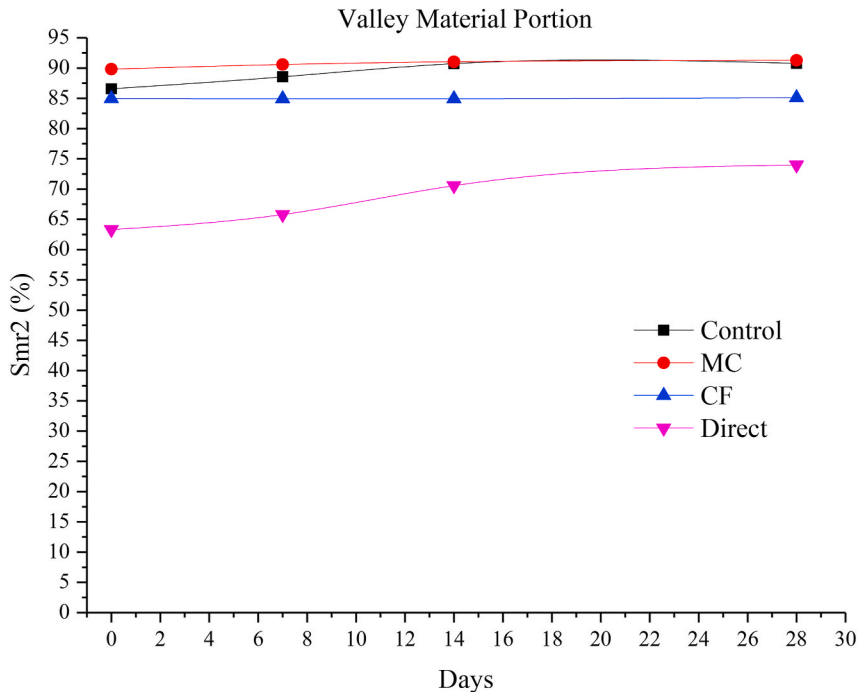

Fig. 14. Valley Material Portion (Smr2-Value) for different concrete mixture.

4.4.2. Root mean square height (Sq-Value)

Root mean square height is equivalent to the standard deviation of heights which represents the ordinate values within the defined area (Eq. (23)) [54], this supports the analyses for further assessment of the height variation statistically (i.e., crack depth). Fig. 13 shows the Root mean square height values during the healing progress for all concrete mixtures at different time intervals. Seemingly, the graphical representation of the Sq-value during the healing performance is similar to the arithmetical mean height with slight variations typically for the concrete mixture 2.5%CF showing the slightly greater healing performance achievement till 14 days (i.e. trend curvature sloping downward toward the right direction) compared to the control mixture where the trend is almost unchanged during the healing progress. This indicates that the cellulose fibers have been effective in self-healing mechanisms (i.e. crack depth becoming shallower). Furthermore, the concrete mixture 5%MC, indicate self-healing has been achievable at 7 days and continuously healing product was obtained till 28 days. For the applied healing agent concrete mixture, the healing performance is significantly achievable from the initial time of the applied healing agent.

$$Sq = \sqrt{\frac{1}{A}\iint_A |Z^2(x,y)| dxdy} \qquad (23)$$

Where Sa is the Arithmetical mean height, A is the surface area and x,y,z are the cartesian coordinates.

4.4.3. Valley material portion (Smr2-Value)

The valley material portion represents the material portion of the reduced valley depth in comparison to the surface which supports the crack valley reduction during the crack healing process [54]. Fig. 14 shows the valley material portion (Smr2-value) for the different concrete mixtures. It can be seen that the healing performance is achieved for all of the concrete mixtures from the (i.e. sloping upward toward the right direction) during the different time intervals. For the control concrete mixture, the valley depth is reduced, based on the Smr2-value the autogenous healing progressed till 14 days by 1.69 % (i.e. increase of Smr2-value from 0 days to 14 days) while the self-healing progress is approximately remained unchanged. These results were also observed in the earlier section. For the concrete mixture 2.5%CF the healing performance is slightly achievable till 14 days, however; further healing has occurred at 28 days the Smr2-value increased by approximately 0.15 %. Similarly, the performance of the self-healing was at low ranges in earlier sections. For the concrete mixture 5%MC, the healing performance is achieved during the 28 days and an increase of Smr2-value of 1.45 % is obtained. It can be noticed that the healing performance of the concrete mixture 5%MC is slightly lower than the control mixture. It can be attributed that the crack healing was also achievable from the crack walls as mentioned in the crack wall closure section which could have the potential to limit obtaining the valley material portion during the scanning progress since the surface texture is through the optical mechanism. Nonetheless, for the concrete mixture where the sodium silicate was applied directly the Smr2-value increased significantly, thus; to 7.23 % and 10.65 % at 14 days and 28 days, respectively. Such an increase in the Smr2-value indicates that the method of applying the healing agent directly on the concrete surface with microcracks has significant healing performance.
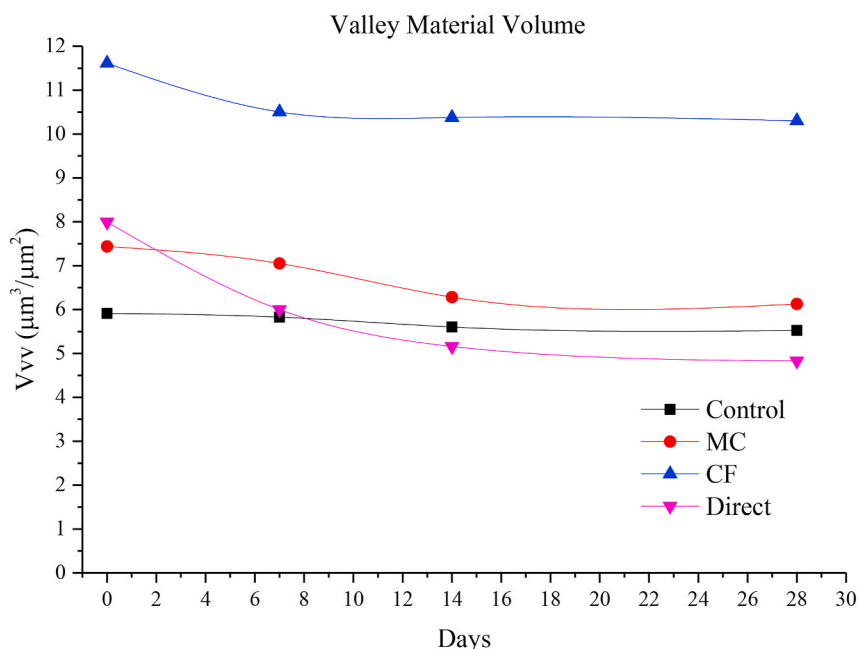

Fig. 15. Dale Void Volume (Vvv-Value) for different concrete mixture.

4.4.4. Dale void volume (Vvv-Value)

The dale void volume represents the void volume of the valley for the area of interest, this parameter is indicative of the healing performance at different time intervals, thus; the reduction in the dale void volume indicates the volumetric content of the healing product [54]. Fig. 15 shows the dale void volume for all concrete mixtures which shows that healing is achievable for all concrete mixtures (i.e. the Vvv-value is sloping downward during the different time intervals). For the control concrete mixture, the volumetric size of the crack is reduced by approximately 0.309 μm^3 till 14 days and further 0.079 μm^3 at 28 days (i.e. total of 0.388 μm^3) due to the autogenous self-healing mechanism. While for the concrete mixture 2.5%CF the self-healing performance progress is achievable and the Vvv-value is reduced by approximately 1.24 μm^3 at 14 days and this performance is reduced to approximately 0.076 μm^3 (i.e. total volumetric size reduced is 1.316 μm^3). For the concrete mixture 5%MC the Vvv-value is reduced by approximately 1.15 μm^3 at 14 days and further reduction of approximately 0.156 μm^3 (i.e. total volumetric size reduced is 1.306 μm^3). The Vvv-value for the concrete mixture where the healing agent (i.e. sodium silicate) applied directly is reduced by approximately 2.84 μm^3 at 14 days and further reduction of 0.33 μm^3 (i.e. total volumetric size reduced by approximately 3.17 μm^3), indicating higher healing performance is achieved.

5. Conclusion

Evaluating the healing performance using non-destructive test methods can be challenging, primarily due to factors such as sample preparation limitations, testing conditions such as vacuum pressures and limitations in obtaining data during test programs, which may result in errors.

In this study, innovative three-dimensional (3D) metrological instrumentation, specifically a surface profiler, was employed to mitigate these limitations in assessing the healing properties of concrete mixtures. The utilization of metrological instruments 3D surface roughness parameters is not frequently employed in analytical applications for cementitious materials, particularly in the context of self-healing applications, due to the high-tech nature of these tools.

The concrete mixtures under investigation included the control mixture, one with 5 % microcapsule content, another with 2.5 % cellulose fibers content, and one with sodium silicate applied directly. The concrete samples had a geometrical size of 40 mm in diameter and 80 mm in height, and they underwent post-crack development through controlled damage equivalent to 70 % of the maximum unconfined compressive strength.

Based on the experimental results the following findings can be withdrawn.

- The addition of healing agents has the potential to enhance the densification properties of concrete mixtures compared to the control mixture, possibly due to the higher powder-to-water ratio, leading to changes in the mechanical property values.
- Surface profiling measurements indicates that self-healing performance is more likely to occur within narrow crack walls and shallow crack depths for autogenous self-healing.
- By using the healing agents, self-healing performance can be achieved in crack walls of different geometrical sizes of widths and depths due to the dispersion of the healing agents which enhance the self-healing performance.
- Similarly, the healing product and contact angle variations demonstrates that self-healing performance is more achievable in crack walls compared to autonomous self-healing from the crack walls and depths.
- It can be attributed that the healing performance is due the chemical reactions and the formation of new cementitious materials, particularly in the concrete mixture containing microcapsules, and potentially, bridge-like connections in the concrete mixture containing cellulose fibers.
- The obtained data from the surface roughness parameters, Sa and Sq values, demonstrates the healing performance across various concrete mixtures and methods of employing healing agents. Evidently the reduction in crack-valley depth, which is calculated as the average and deviation of the peak and valley (since the peak remains unchanged).
- Also, the Smr2 and Vvv values exhibit an inverse mechanism, where a reduction in the Smr2 value indicating a reduction in the valley portion, leads to greater self-healing achievement.

The use of metrological instrumentation and the 3D profiler is a promising testing method for evaluating self-healing performance and efficiency in cementitious materials. The selection of roughness parameters for assessing self-healing performance has the potential to impact the evaluation of healing efficiency However, there are certain limitations inherent in surface texture scanning and analysis techniques, including: 1) data gaps for pore/crack depths exceeding the detection depth (e.g., greater than 950 μm), and 2) limitations in sectioning, involving the identification of 31 points along the crack's length at different time intervals.

CRediT authorship contribution statement

Amir Sidiq: Writing – original draft, Software, Methodology, Investigation, Formal analysis, Data curation, Conceptualization. **Sujeeva Setunge:** Methodology, Conceptualization, Writing – review & editing. **Pratheep Kumar Annamalai:** Conceptualization, Methodology, Writing – review & editing. **Rebecca J. Gravina:** Conceptualization, Methodology, Writing – review & editing. **Filippo Giustozzi:** Conceptualization, Funding acquisition, Methodology, Project administration, Resources, Supervision, Writing – review & editing.

Declaration of competing interest

The authors declare that they have no known competing financial interests or personal relationships that could have appeared to

influence the work reported in this paper.

Data availability

Data will be made available on request.

References

[1] S. Qaidi, et al., 3D printed geopolymer composites: a review, Mater. Today Sustain. 20 (2022) 100240, https://doi.org/10.1016/j.mtsust.2022.100240.
[2] Available from:, Activity Report_2017_Cembureau, 2019 https://cembureau.eu/media/1716/activity-report-2017.pdf.
[3] Global cement production top countries 2017 | Statistic, Available from: https://www.statista.com/statistics/267364/world-cement-production-by-country/, 2018.
[4] T.H. Nguyen, et al., Bacterial self-healing of concrete and durability assessment, Cement Concr. Compos. 104 (2019) 103340, https://doi.org/10.1016/j.cemconcomp.2019.103340.
[5] V.C. Li, On engineered cementitious composites (ECC) A review of the material and its applications, J. Adv. Concr. Technol. 1 (3) (2003) 215–230, https://doi.org/10.3151/jact.1.215.
[6] A. Sidiq, et al., Microstructural analysis of healing efficiency in highly durable concrete, Construct. Build. Mater. 215 (2019) 969–983, https://doi.org/10.1016/j.conbuildmat.2019.04.233.
[7] A. Sidiq, R. Gravina, F. Giustozzi, Is concrete healing really efficient? A review, Construct. Build. Mater. 205 (2019) 257–273, https://doi.org/10.1016/j.conbuildmat.2019.02.002.
[8] B. Aytekin, A. Mardani, Ş. Yazıcı, State-of-art review of bacteria-based self-healing concrete: Biomineralization process, crack healing, and mechanical properties, Construct. Build. Mater. 378 (2023) 131198, https://doi.org/10.1016/j.conbuildmat.2023.131198.
[9] C. Joseph, et al., Experimental investigation of adhesive-based self-healing of cementitious materials, Mag. Concr. Res. 62 (11) (2010) 831–843, https://doi.org/10.1680/macr.2010.62.11.831.
[10] F.A. Gilabert, et al., Integral procedure to assess crack filling and mechanical contribution of polymer-based healing agent in encapsulation-based self-healing concrete, Cement Concr. Compos. 77 (Supplement C) (2017) 68–80, https://doi.org/10.1016/j.cemconcomp.2016.12.001.
[11] I. Karatas, Microbiological Improvement of the Physical Properties of Soils, Arizona State University, 2008.
[12] K. Vijay, M. Murmu, S.V. Deo, Bacteria based self healing concrete – a review, Construct. Build. Mater. 152 (2017) 1008–1014, https://doi.org/10.1016/j.conbuildmat.2017.07.040.
[13] A. Kanellopoulos, T.S. Qureshi, A. Al-Tabbaa, Glass encapsulated minerals for self-healing in cement based composites, Construct. Build. Mater. 98 (Supplement C) (2015) 780–791, https://doi.org/10.1016/j.conbuildmat.2015.08.127.
[14] J.J. Chen, et al., Solubility and structure of calcium silicate hydrate, Cement Concr. Res. 34 (9) (2004) 1499–1519, https://doi.org/10.1016/j.cemconres.2004.04.034.
[15] P. Giannaros, A. Kanellopoulos, A. Al-Tabbaa, Sealing of cracks in cement using microencapsulated sodium silicate, Smart Mater. Struct. 25 (8) (2016) 084005. https://10.1088/0964-1726/25/8/084005.
[16] N.Z. Muhammad, et al., Tests and methods of evaluating the self-healing efficiency of concrete: a review, Construct. Build. Mater. 112 (2016) 1123–1132, https://doi.org/10.1016/j.conbuildmat.2016.03.017.
[17] A. Lorenzi, F.T. Tisbierek, L. Silva, Ultrasonic pulse velocity análisis in concrete specimens, in: IV Conferencia panamericana de end, 2007 *buenos aires*.
[18] ASTM-C597, C597 - 16, Standard Test Method for Pulse Velocity through Concrete, ASTM International, 2016.
[19] S. Popovics, J.L. Rose, J.S. Popovics, The behaviour of ultrasonic pulses in concrete, Cement Concr. Res. 20 (2) (1990) 259–270, https://doi.org/10.1016/0008-8846(90)90079-D.
[20] S. Granger, et al., Experimental characterization of the self-healing of cracks in an ultra high performance cementitious material: mechanical tests and acoustic emission analysis, Cement Concr. Res. 37 (4) (2007) 519–527, https://doi.org/10.1016/j.cemconres.2006.12.005.
[21] K. Van Tittelboom, et al., Acoustic emission analysis for the quantification of autonomous crack healing in concrete, Construct. Build. Mater. 28 (1) (2012) 333–341, https://doi.org/10.1016/j.conbuildmat.2011.08.079.
[22] S. Mukherjee, S. Mandal, U. Adhikari, Healing of micro-cracks in fly Ash cement composite using NaOH and Na2SiO3 solution, i-Manager's J. Struct. Eng. 6 (3) (2017) 37, https://doi.org/10.26634/jste.6.3.13733.
[23] X. Wang, et al., Object status identification of X-ray CT images of microcapsule-based self-healing mortar, Cement Concr. Compos. 125 (2022) 104294, https://doi.org/10.1016/j.cemconcomp.2021.104294.
[24] S.-Y. Chung, et al., Overview of the use of micro-computed tomography (micro-CT) to investigate the relation between the material characteristics and properties of cement-based materials, Construct. Build. Mater. 229 (2019) 116843, https://doi.org/10.1016/j.conbuildmat.2019.116843.
[25] A. Sidiq, et al., High-efficiency techniques and micro-structural parameters to evaluate concrete self-healing using X-ray tomography and Mercury Intrusion Porosimetry: a review, Construct. Build. Mater. 252 (2020) 119030, https://doi.org/10.1016/j.conbuildmat.2020.119030.
[26] J. Van Stappen, et al., The microstructure of capsule containing self-healing materials: a micro-computed tomography study, Mater. Char. 119 (2016) 99–109, https://doi.org/10.1016/j.matchar.2016.07.014.
[27] Ł. Sadowski, et al., New paradigm in the metrology of concrete surface morphology: methods, parameters and applications, Measurement 169 (2021) 108497, https://doi.org/10.1016/j.measurement.2020.108497.
[28] Ł. Sadowski, T.G. Mathia, Multi-scale metrology of concrete surface morphology: fundamentals and specificity, Construct. Build. Mater. 113 (2016) 613–621, https://doi.org/10.1016/j.conbuildmat.2016.03.099.
[29] T. Ficker, D. Martišek, H.M. Jennings, Roughness of fracture surfaces and compressive strength of hydrated cement pastes, Cement Concr. Res. 40 (6) (2010) 947–955, https://doi.org/10.1016/j.cemconres.2010.02.002.
[30] R. Ourahmoune, et al., Surface morphology and wettability of sandblasted PEEK and its composites, Scanning: J. Scanning Microsc. 36 (1) (2014) 64–75. https://10.1002/sca.21089.
[31] T. Ficker, D. Martišek, Digital fracture surfaces and their roughness analysis: applications to cement-based materials, Cement Concr. Res. 42 (6) (2012) 827–833, https://doi.org/10.1016/j.cemconres.2012.03.007.
[32] Y. Liu, et al., Full-field 3D shape measurement of discontinuous specular objects by direct phase measuring deflectometry, Sci. Rep. 7 (1) (2017) 10293. https://10.1038/s41598-017-11014-5.
[33] S. Thian, et al., Dimensional Measurement of 3D Microstruture Based on White Light Interferometer, in: Journal of Physics: Conference Series, IOP Publishing, 2007.
[34] P. Pavliček, E. Mikeska, White-light interferometer without mechanical scanning, Opt Laser. Eng. 124 (2020) 105800. https://10.1016/j.optlaseng.2019.105800.
[35] P. de Groot, Principles of interference microscopy for the measurement of surface topography, Adv. Opt Photon 7 (1) (2015) 1–65. https://10.1364/AOP.7.000001.
[36] I. Kassamakov, et al., 3D super-resolution optical profiling using microsphere enhanced Mirau interferometry, Sci. Rep. 7 (1) (2017) 3683. https://10.1038/s41598-017-03830-6.
[37] J.F. Biegen, Interferometric Surface Profiler for Spherical Surfaces, 1990. Google Patents.
[38] P. Hariharan, Basics of Interferometry, Elsevier, 2010.

[39] S. Thian, et al., Dimensional measurement of 3D microstruture based on white light interferometer. in, in: Journal of Physics: Conference Series, IOP Publishing, 2007.

[40] Creath, K., Step height measurement using two-wavelength phase-shifting interferometry. Appl. Opt. 2614198728102816 ; [e-reference] https://10.1364/ AO.26.002810;.

[41] R. Leach, Optical Measurement of Surface Topography, 8, Springer, 2011.

[42] D. Wu, F. Fang, Development of surface reconstruction algorithms for optical interferometric measurement, Front. Mech. Eng. 16 (2021) 1–31, https://doi.org/ 10.1007/s11465-020-0602-6.

[43] General Purpose and Blended Cement, 2018.

[44] A. Sidiq, et al., Self-repairing cement mortars with microcapsules: a microstructural evaluation approach, Construct, Build. Mater. 232 (2020) 117239., https:// doi.org/10.1016/j.conbuildmat.2019.117239.

[45] K.N.M. Amin, et al., Production of cellulose nanocrystals via a scalable mechanical method, RSC Adv 570 (2015) 57133–57140, https://doi.org/10.1039/ C5RA06862B.

[46] AS-1012.8.4:2015, Methods of Testing Concrete Method, 2018, www.saiglobal.com.

[47] J. Hu. Porosity of Concrete-Morphological Study of Model Concrete, 2004.

[48] A. Sidiq, et al., Microstructural analysis of healing efficiency in highly durable concrete, Construct. Build. Mater. 215 (2019) 969–983, https://doi.org/10.1016/ j.conbuildmat.2019.04.233.

[49] H. Singh, R. Gupta, Influence of cellulose fiber addition on self-healing and water permeability of concrete. Case Stud, Construct. Mater. 12 (2020) e00324. http://hdl.handle.net/1828/11634.

[50] M. Bentchikou, et al., Effect of recycled cellulose fibres on the properties of lightweight cement composite matrix, Construct. Build. Mater. 34 (2012) 451–456, https://doi.org/10.1016/j.conbuildmat.2012.02.097.

[51] D. Snoeck, N. De Belie, Mechanical and self-healing properties of cementitious composites reinforced with flax and cottonised flax, and compared with polyvinyl alcohol fibres, Biosyst. Eng. 111 (4) (2012) 325–335, https://doi.org/10.1016/j.biosystemseng.2011.12.005.

[52] J.O. Okeniyi, et al., Probability density fittings of corrosion test-data: implications on C6H15NO3 effectiveness on concrete steel-rebar corrosion, Sadhana 39 (3) (2014) 731–764. https://10.1007/s12046-014-0226-9.

[53] ISO 25178-6:2010 Geometrical Product Specifications (GPS) — Surface Texture: Areal — Part 6: Classification of Methods for Measuring Surface Texture.

[54] Introduction to Surface Roughness Measurement.